CHALMERS

Measurement Techniques for Identifying Polarity of Ion Injection in Transformer Oil

Master of Science Thesis in Electric Power Engineering

DEEPTHI KUBEVOOR RAMESH

Department of Materials and Manufacturing Technology
CHALMERS UNIVERSITY OF TECHNOLOGY
Gothenburg, Sweden, 2012
Diploma Work No. 88/2012

Measurement Techniques for Identifying Polarity of Ion Injection in Transformer Oil

by

DEEPTHI KUBEVOOR RAMESH

Diploma work No. 88/2012
Department of Materials and Manufacturing Technology
CHALMERS UNIVERSITY OF TECHNOLOGY
Gothenburg, Sweden

Diploma work in the Master Program in Electric Power Engineering

Performed at: ABB Corporate Research
SE- 721 78 Västerås, Sweden

Supervisor: Dr. Joachim Schiessling
ABB Corporate Research
SE- 721 78 Västerås, Sweden

Examiner: Associate Professor**.** Yuriy Serdyuk
Department of Materials and Manufacturing Technology
Chalmers University of Technology
SE- 412 96 Gothenburg, Sweden

Measurement techniques for identifying polarity of ion injection in transformer oil
DEEPTHI KUBEVOOR RAMESH

Diploma work No: 88/2012
Department of Materials and Manufacturing Technology
Chalmers University of Technology
SE-412 96 Gothenburg
Sweden
Telephone + 46 (0)31-772 1000

Cover:
International conference & exhibition on VSC technology for HVDC & FACTS, CPRI, India 2012
ABB, 800 kV UHVDC converter transformer

Chalmers Reproservice
Gothenburg, 2012

Measurement techniques for identifying polarity of ion injection in transformer oil

DEEPTHI KUBEVOOR RAMESH

Department of Materials and Manufacturing Technology
Division of High Voltage Engineering
Chalmers University of Technology

Abstract

For transferring large amount of power over long distance, the most preferred technology is High Voltage Direct Current (HVDC) transmission. This is not only the cheapest technique, but also a more environment friendly. The major component for such long distance transmissions is a DC converter that is fed from a power transformer. Due to higher ratings, the insulation system of such transformers must be able to handle DC and AC electric stresses.

The insulation in large DC converter transformer normally consists of oil and cellulose material. Application of DC voltage in such a system causes dissociation of oil molecules leading to space charge buildup and its accumulation on the surface of the insulation. The space charge free AC field can be calculated easily with the help of numerical methods while obtaining the space charge dependent DC field is a challenge since they are conditioned by dynamics of charges defined by their mobilities and injection from insulation components.

The main task of the present project was to investigate the polarity dependence on ion injection.

To achieve this, experimental setups of different geometries were used to measure current in oil at different applied voltages. Two different approaches, namely so called single polarity method and polarity reversal method were utilized in the measurements. The steady currents obtained with the different techniques were analyzed to identify the polarity of ion injection. Further the measured currents were compared with the results of simulations (subject of another person) to observe the trends.

The results from the measurements performed with the different geometries indicated that there was a polarity dependence of the intensity of ion injection. However it was found that the sign of injected ions was positive in all the set-ups used.

Another observation was the dependence of the current on grounding time in-case of single polarity measurements. It was clearly observed that the minimum time for the set-up to reach a state of equilibrium was in the order of days while minutes and hours led to local maxima in the recorded current traces.

Keywords: ion drift model, transformer oil, single polarity method, polarity reversal, grounding, UHVDC transformer, ion injection, resistivity

Acknowledgements

This Master thesis work was carried out from January to June 2012 in co-operation between the ABB Corporate Research, Västerås, Sweden and the Division of High Voltage Engineering at Chalmers University of Technology, Göteborg, Sweden.

It would have never been possible without guidance, support and encouragement from many people.

First I would like to express my deepest gratitude to my supervisor Dr. Joachim Schiessling (ABB Corporate Research) for the patience and help. His broad knowledge, understanding and personal guidance helped me to then learn and to analyze a lot of new things during the work. I would also like to thank Dr. Olof Hjortstam for fruitful discussions and new ideas that helped me to explore more interesting and new things throughout the work. I am grateful to Leif A Pettersson for being a wonderful manager and showing interest in the progress of my thesis at ABB, CRC. I express my sincere gratitude to all the people in the ELD and IMT group and employees at ABB CRC for the new ideas and suggestions. Thanks to ABB Corporate research for providing me with a good working environment.

I am also indebted to Assoc. Prof. Yuriy Serdyuk (Chalmers) for the regular feedbacks and motivation during the time of my thesis work and also for being my examiner at Chalmers University of Technology.

During the work I collaborated with many colleagues for whom I have a great regard. I wish to extend my warmest thanks to Christian Sonehag for providing me with simulation results and discussions that helped me understand and improve my work in a better way and also my other master thesis colleagues at the ABB CRC for making the working environment very comfortable to work.

My sincere thanks to Chalmers University of Technology for providing me with an opportunity to do my Master studies in Sweden. Many thanks to everyone in the Department of Electric Power Engineering and Division of High Voltage Engineering for providing me with an education that helped me to develop my theoretical and practical skills.

Finally I would like to thank my parents for letting me travelling 5000 miles to do my Master studies abroad and to acquire a wonderful education. My heartfelt gratitude to my other family members, Indian and international friends for never making me feel lonely and for always being there when I needed the most.

Göteborg
June 2012
Deepthi Kubevoor Ramesh.

Table of Contents

.

1. INTRODUCTION

An increase in the energy demand and advances in the environmental policies have made a significant impact on the developments of innovative applications and technical improvements in the field of HVDC transmission. This type of power transportation has not only environmental advantages, but it is also very economical when it comes to long distances. In particular, this is the most preferred technology for utilizing energy from renewable sources (hydro, solar, etc.) located very far away from the load centers.

This technology has been used for more than 50 years now. It is more reliable and valuable than HVAC transmission systems. It has been growing rapidly around the world. One of the major HVDC projects in the recent years has been the development of 800 kV UHVDC link which covers a distance of 1700 km from central India. When operating at full capacity, it can supply electricity to 90 million people [1]. One of the main elements of such system is a DC converter that is fed from a power transformer (Figure 1). This transformer has to be made for a higher rating to satisfy the required demands. As the cost increases with the size of the system, it has to be made more compact. Due to the higher ratings, these transformers are subjected to higher AC and DC electric stress based on the voltage levels [1]. The insulation system of the transformers has to be made to handle high stresses. It is a combination of solid insulation and mineral oil. The insulation and the oil have different dielectric properties, conductivities and permittivity. The oil is more conductive and has a lower permittivity than the solid insulation. Due to this fact, there is a different field distribution in the system under the application of AC and DC voltage. Application of DC voltage causes dissociation of the ions in the transformer oil that leads to a space charge accumulation on the surface of the insulation.

Figure 1. 800kV HVDC transformer& Developments in India.

(photographs: ABB& CLSA Asia Pacific Market)

The main idea of the thesis was to investigate the polarity of ion injection using test cells with different geometries. At first the resistivity of the mineral oil was measured at different temperatures and using different cleaning procedures. Further, voltage-current measurements using single polarity and polarity reversal method for different experimental set-ups with metal electrodes were performed.

The structure of the report is as follows. Chapter 2 discusses existing physical models of charge transport in insulating oil (so-called ion drift model) and ion injection on metal-liquid interfaces based on concept of an- electrical double layer. Chapter 3 is about the instruments and equipment used for measurement of both resistivity and current in the insulation. It contains a description of cleaning procedures used for different test cells as well as a presentation of the results of the resistivity measurements. Chapter 4 provides information about the resistivity measurements for oils from different experimental set-up. Chapter 5 is about voltage-current measurements utilizing single polarity and polarity reversal methods and stresses the importance of the grounding time in the measurements and presents an evaluation of the obtained results. In the discussion in chapter 6, the experimental results are compared with simulations and possible physical explanations behind the injection phenomenon and its polarity dependence are proposed. Finally it concludes the work done and proposals for future activities that may provide deeper knowledge in the subject.

2. PHYSICS OF CHARGE TRANSPORT AND INJECTION IN OIL

2.1 Ion drift diffusion model

For designing a consistent HVDC transformer, the insulation system should withstand AC and DC stresses. In general these stresses are of dynamic character even at DC since the insulation is exposed to a constant DC voltage as well as to, the voltage variations during turn on, turn off and polarity reversal. The latter affects the insulation system at most because the fields induced by accumulated charges are superimposed with the applied fields. Due to this phenomenon, extremely strong electric field may appear at certain parts of the insulation system. Evaluations of the field levels under such conditions are challenging. Thus the space charge free AC field can be calculated relatively easy with the help of numerical methods. The situation is different for DC as space and surface charges cannot be excluded from the consideration and their dynamic behavior should be taken into account [3]. In addition, dependencies of materials properties (permittivities, conductivities, etc.) on temperature, moisture content and aging should be accounted for.

Transformer oil is a main part of HVDC transformer insulation. It is considered to be a weak electrolyte where the ions and ion pairs are dissolved [4]. They dissociate to form ions from a constant background density of ion pairs which can be transported in the electric field or can also recombine to form neutral molecules [3]. When a DC voltage is applied to a non-polar liquid, conduction takes place because of the drift of ions in the liquid itself ('residual conduction') or because of the ions created at the electrode ('injection') [5].

According to Bjerrum's theory, in a weak electrolyte like transformer oil, only a minor part of ion pair dissociate due to low permittivity whereas the majority of the ions are associated to form ion pairs due to the electrostatic forces [6].

Thomson model of ionic conduction in gases is the starting point of the conduction model in dielectric fluids [7]. Conduction process is controlled by two mechanisms: dissociation of neutral molecules into ionic species and their recombination back to neutral molecule [8]:

$$AB \underset{k_2}{\overset{k_1}{\rightleftharpoons}} A^+B^- \underset{k_R}{\overset{k_D}{\rightleftharpoons}} A^+ + B^- \qquad (1)$$

Here A^+B^- is the neutral ion pair formed by the two ions A and B. A^+ and B^- are the free ions dissociated from the neutral pair A^+B^-. k_1, k_2 are the kinetic constants ; k_D, k_R are the dissociation and recombination constants respectively. k_D is field dependent and k_R is field invariant.

Similar description is used in case of injection of charge carriers from a metal electrode which involves creation of charge carriers and extraction of ions. Hence conduction in oil may appear due to unipolar injection of ions at high electric fields and due to dissociation of oil molecules and injection at low electric fields [9].

In general, dynamics of ions in oil is governed by the rate equation [10, 11]

$$\frac{dp}{dt} = \frac{dn}{dt} = k_D c - k_R pn \tag{2}$$

where p and n are the densities of positive and negative ions and c is the density of the ion pairs. At thermodynamic equilibrium, the density of the positive and the negative ions are equal and are much lower than the ion pair density. Then they are defined by the conductivity of the material as

$$p_0 = n_0 = \frac{\sigma}{q(\mu_p + \mu_n)} \tag{3}$$

Here q is the elementary charge, μ_p and μ_n are the mobilities of positive and negative ions respectively.

The recombination constant is expressed by Langevin expression as [12]

$$k_R = \frac{q(\mu_p + \mu_n)}{\varepsilon_0 \varepsilon_r} \tag{4}$$

which does not depend on the electric field, ε_0 is 8.854 * 10^-12 C/V-m and ε_r is the relative permittivity of the material. The dissociation constant is field dependent and is given by Onsager theory [13],

$$k_D = k_D^0 F(E) = k_D^0 \frac{I_1(4b)}{2b} \tag{5}$$

$$b = \sqrt{\frac{q^3 E}{16\pi\varepsilon_0\varepsilon_r k^2 T^2}} \tag{6}$$

where I1 is the modified Bessel function of the first kind and order one, kis the Boltzmann constant, q is charge and T is the absolute temperature.

At high electric fields, the concentration of free ions increases and so does the conductivity of the liquid [14]. In thermal equilibrium and at no applied field equation (2) becomes,

$$k_D^0 = k_R \frac{n_0^2}{c} \tag{7}$$

When an external electric field is applied, the charge carriers are separated due to the electrostatic forces and move towards the electrode having opposite sign of the

applied potential. They experience drift and diffusion and their drift velocity can be defined by their mobility.

$$\vec{w}_{p,n} = \mu_{p,n}\vec{E} \tag{8}$$

The applied electric field causes diffusion of ions due to the buildup of ion distribution. The diffusive fluxes of the ions are proportional to the gradient of the ions densities. The diffusion coefficients are defined by Einstein's relation is

$$D_{p,n} = \frac{kT}{q}\mu_{p,n} \tag{9}$$

Including the ion drift and diffusion term to equation (2) and also using equation (7) would give

$$\begin{cases} \dfrac{\partial p}{\partial t} + \nabla\left(\mu_p \vec{E} p - D_p \nabla p\right) = k_R n_0^2 F(E) - k_R p n \\ \dfrac{\partial n}{\partial t} - \nabla\left(\mu_n \vec{E} n + D_n \nabla n\right) = k_R n_0^2 F(E) - k_R p n \end{cases} \tag{10}$$

where F(E) is the field enhancement of the dissociation. The concentrations of ions may be high enough to create strong electric field (even comparable with the applied one) and, hence, the equations (10) should be complemented with Poisson's equation to form a self-consistent model:

$$\nabla(\varepsilon_0 \varepsilon_r \nabla\phi) = -q(p - n), \qquad \vec{E} = -\nabla\phi \tag{11}$$

The macroscopic ionic current density is obtained from the concentrations of free ions, electric intensity and charge mobility. It is defined as

$$J_p = q\left(\mu_p \vec{E} p - D_p \nabla p\right), \qquad J_n = q\left(\mu_n \vec{E} n - D_n \nabla n\right), \qquad J_{ion} = J_p + J_n \tag{12}$$

The displacement current (due to the geometrical capacitance of the system) is due to the change in the electric field and has contribution from moving charges towards the opposite electrode and sudden change of applied field

$$\vec{J}_{displacement} = \frac{\partial \vec{D}}{\partial t} = \varepsilon_0 \varepsilon_r \frac{\partial \vec{E}}{\partial t} \tag{13}$$

Hence the total current density is given by the summation of the ionic current density and displacement current density.

$$\vec{J}_{tot} = \vec{J}_{ion} + \vec{J}_{displacement} \tag{14}$$

The total current is obtained by integrating the total current density over the surface of the electrode.

The current curve gives the overall information about the residual conduction and the charge injection.

2.1.1 Relevant time scale for current measurement

Currents in oil are usually measured as a response to a certain applied voltage. As shown above, the current is in general time dependent and, therefore, parameters describing its time variations are to be defined. Since the ionic current is of main interest in the present study, relevant definitions are provided below

2.1.1.1 Transit time

This is the mean time for an ion to migrate between the two electrodes. It depends on geometry of the electrodes, the mobility of the ions and the applied voltage.

The transit time is given by

$$t_{transit} = \int_{electrode\ 1}^{electrode\ 2} \frac{1}{\mu_{p,n}\left|\vec{E}\right|} ds \tag{15}$$

Thus in case of parallel plate geometry the transit time equals to

$$t_{transit} = \frac{d}{\mu_{p,n}\frac{|V|}{d}} = \frac{d^2}{\mu_{p,n}|V|} \tag{16}$$

Here V is the voltage applied over the electrodes and d the distance between them.

In the case of a coaxial geometry, the electric field behaves like

$$E(r) = \frac{V}{r\log\frac{r_{outer}}{r_{inner}}} \tag{17}$$

where r_{outer} and r_{inner} are the radiuses of the outer and inner electrodes respectively. Integrating this over r to get the transit time yields

$$t_{transit} = \int_{inner\ electrode}^{outer\ electrode} \frac{r\log\frac{r_{outer}}{r_{inner}}}{\mu_{p,n}\left|U_{app}\right|} dr$$

$$t_{transit} = \frac{(r_{outer}^2 - r_{inner}^2)\log\frac{r_{outer}}{r_{inner}}}{2\,.\,\mu_{p,n}\left|U_{app}\right|} \tag{18}$$

The final expression (18) is to be used below since the measurements were performed in coaxial electrode systems.

2.1.1.2 Relaxation time

This is the mean time between collisions at the thermodynamic equilibrium or in other words the measure of how fasts the ions will relax after their removal of the applied voltage. This time is given by

$$t_{relax} = \varepsilon_0 \varepsilon_r \rho \tag{19}$$

where ρis the resistivity of oil and ε_r is its dielectric constant (~4.2).

2.1.1.3 Conduction characterization parameter Co

This parameter decides the regime of conduction imposed by the dissociation of ion pairs. It is the ratio between the transit time and the relaxation time. For the parallel plate geometry, it is given by

$$C_0 = \frac{q n_0(0) d^2}{\varepsilon V} \tag{20}$$

and in the case of a coaxial geometry, it is

$$C_0 = \frac{q n_0 (r_{outer}^2 - r_{inner}^2) \log \frac{r_{outer}}{r_{inner}}}{\varepsilon_0 \varepsilon_r V} \tag{21}$$

When C_0>> 1, a quasi-ohmic regime appears where the rate of generation of free ions from ion pairs is equal to the rate of recombination. Here the relaxation time is much faster than the transportation time and the equilibrium is slightly perturbed by the electric field. A voltage- current characteristic illustrating this regime is shown in Figure 2.

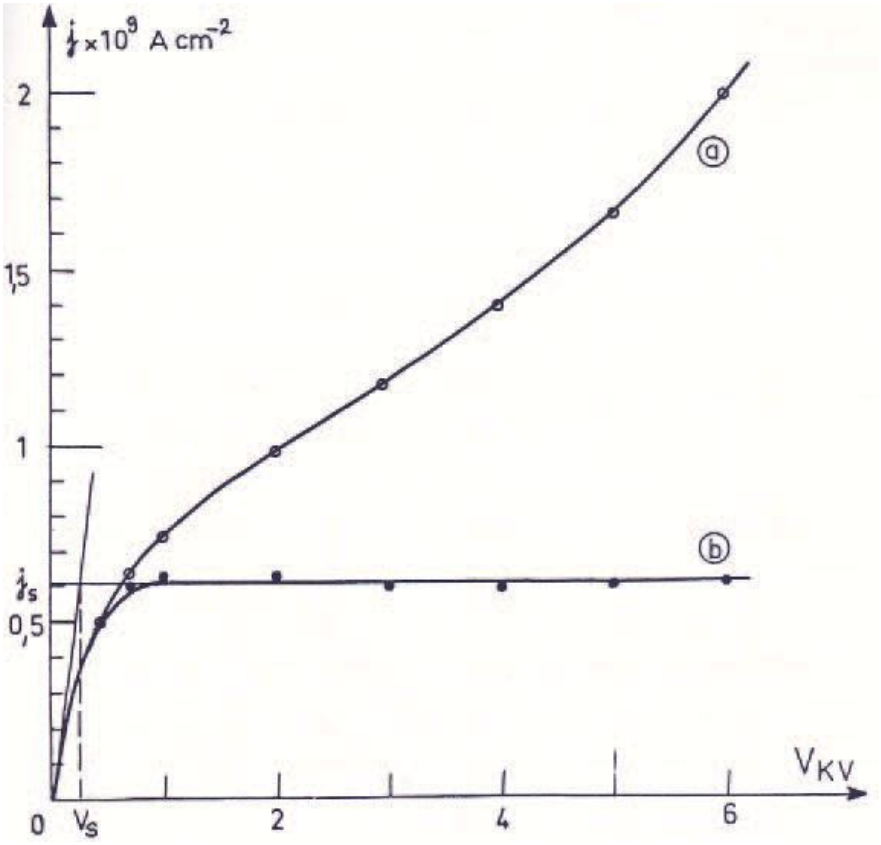

Figure 2. Thomson-Onsager current-voltage characteristic for cyclohexane. Curve (a) current density j(V) and Curve (b) ratio j/ F(E) [16].

The case with $C_0 << 1$, corresponds to the saturation regime where the dissociation or recombination equilibrium is destroyed and the current density is limited by the dissociation process. [11, 15, 16].

It is to be observed that C_0 is the same as κ and both define the ratio of transit time to the relaxation time [3].

2.2 Electrical double layer

When a charged metallic surface of the electrode is present in a electrolyte solution (oil), there is a rearrangement of ions distribution near the metal surface and a formation of an electrode layer called electrical double layer [17].

It consists of so-called surface layer of ions of one polarity that are adsorbed on the conducting surface directly. The adsorption is mainly due to chemical interactions and the polarity of the ions on the surface of the electrodes is defined by properties of the liquid-electrode interface. This layer of ions is rigidly bound to the surface of the metal electrode and is also called as Stern layer. In Figure 3, the polarity of the rigid ions is assumed to be negative.

The second layer is formed by loosely bound ions that are attracted due to Coulomb force to the rigid layer (Stern or surface layer). The ions within this

region move due to the influence of applied electric field. This layer is called the diffusive layer [18].

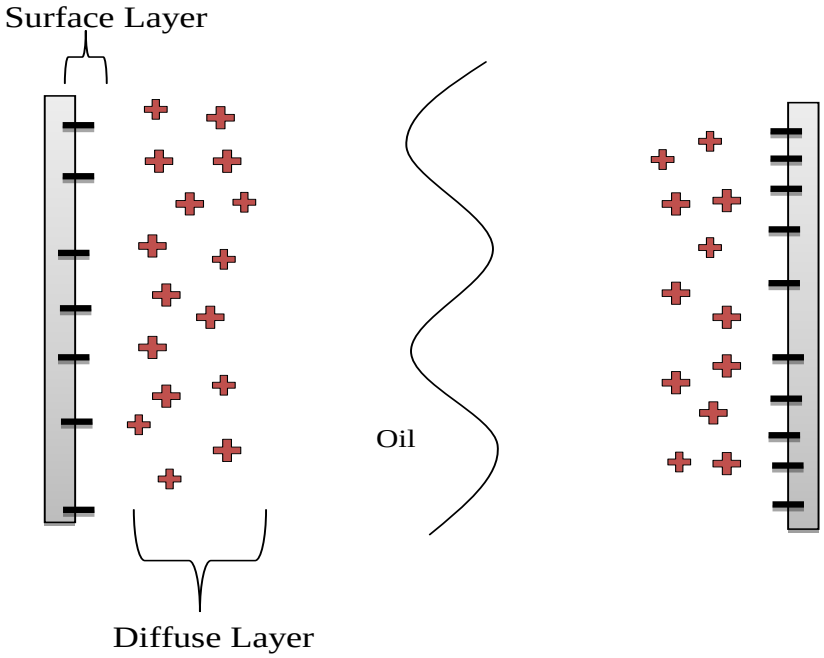

Figure 3. Formation of the electrical double layers in oil near the electrodes.

2.3 Ion injection

Usually, the process of charge transfer takes place on surfaces with opposite sign of the potential as that of the charge to be transferred. In contrast, the injection takes place on the surface with the same sign of the potential as that of the charge of the injected ions. At present the details of the mechanisms have not been clearly understood [10]. The injection of ions is described in three steps:

1) Ionic pairs are attached to the metal surface by the electrostatic image force
2) Dissociation of ion pairs occurs due to the charge transfer reaction between the metal and the ionic pairs. (this also causes oxidation or reduction of one of the ions from the ionic pair).
3) The other ion from the ionic pair can be extracted from the interface by the Schottky effect [9]

The expression for injected charge density by considering the charges extracted by the Schottky effect is given by

$$q_i = \frac{q_i^0}{2b\, K_i(2b)} \tag{22}$$

where q_i^0 is a constant and K_i is the modified Bessel function of the second kind and first order. This equation can be used for both positive and negative injection. As explained above the injection is originated from the ionic pairs absorbed on the

metal surface and hence q_i^0 is related to the residual conductivity of the liquid. Using the above assumptions, a dimensionless constant can be defined

$$A = \frac{q_i^0}{\sigma/(K_+ + K_-)} = \frac{q_i^0}{e_0 n_0} \tag{23}$$

where e_0 is the absolute value of electronic charge [11].

2.3.1 Injection characterization parameter C

The strength of the injection is given by the parameter C in case unipolar injection. The parameter is given by

$$C = \frac{q_i(0)d^2}{\varepsilon V} \tag{24}$$

where qi(0) is the injected charge density given by the equation (22). The values of C<< 1 correspond to a weaker injection without any interference with the electric field and for C>> 1 the injection is stronger and the electric field distribution is affected by the injected charge [11, 15].

2.2.2 Injection of ions from the electrical double layer

Ion injection can be described as the transfer reaction of ion pairs near the electrodes [11]. The ion pairs are attached due to the electrode by electrostatic image force. As described earlier, the ions pair will be dissociated and reduction/oxidation of one of the ion in the pair occurs due to the charge transfer reaction. The other ion will become a part of the diffusive layer and can be injected into the bulk of the oil [9], Figure 4. Assuming that the diffusive layer is negative, the following reaction occurs,

$$A^+B^- + e^- \rightarrow A + B^- \tag{25}$$

Here A^+ and B^- are assumed to be the same ions as in equation (1) which means that they can take part in recombination reactions with the ions in the bulk.

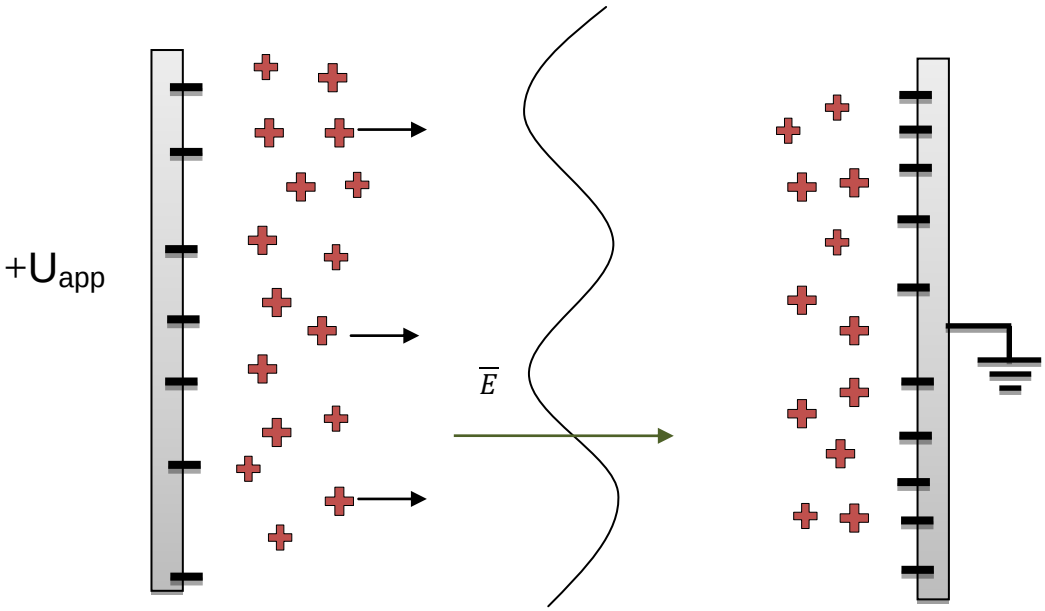

Figure 4. Electrical double layer injecting ions.

2.2.3 Polarity of ion injection

The polarity of the rigid or diffusive layer of the electrical double layer would help to obtain the polarity of the ion injection. To determine this, one of the approaches used it to perform voltage-current measurements in different set-ups providing different field conditions, as suggested in [5]. Hence with the help of the electrode with the lowest electric field, we can determine the sign of injection. This is done by identifying the injecting electrode. This approach is explained further on.

2.2.4 Ion injection from electrodes

Assuming that the generation of ions from the diffusive layer is much faster than the injection, the expression for the injected charge density due to the escape of ions from the double layer is given by

$$n_{inj} = An_0 F_i(E) = An_0 \frac{1}{2bK_1(2b)} \tag{26}$$

where K_1 is the modified Bessel function of the second kind and order one ; A is a constant found to be in the order of unity in most of dielectric liquids [11]. The expression for b defined in (6) and it should be evaluated at the injecting electrode. Using (3), the above equation (26) can be rewritten as

$$n_{inj} = \frac{A\sigma}{q(\mu_p + \mu_n) \cdot 2bK_1(2b)} \tag{27}$$

From the expression for the injected charge density, the injected current density can be determined as

$$\tilde{J}_{inj} = q\mu n_{inj}\tilde{\bar{E}}_{sur} \tag{28}$$

where μ stands for the mobility of the injected ions in the oil and $\tilde{\bar{E}}_{sur}$ is the electric field at the surface of the injecting electrode.

3. EXPERIMENTAL SET-UP AND PROCEDURES

This chapter is about the types of experimental set-ups and the other instrumentation that were used to measure resistivity and also electric currents with single and polarity reversal methods. It also explains different cleaning procedures of oil samples.

3.1 Test cells for resistivity measurement

The resistivity of the oil was measured by applying a very low AC voltage (2 V) to avoid the ions sweep-out effect. Figure 5 (a) and 5 (b) show the test cells used for the measurements. After cleaning the cells according to defined procedures (explained in chapter 3.4), they were filled with oil and connected to the measuring system. The cells indicated as IR1 and IR2 [19] in Figure 5 had 20 ml and 200 ml volume, respectively. The high voltage terminal of the measuring system was connected to the voltage input and the low voltage terminal of the measuring system is connected to the signal output terminal of the test cells.

The hardware used for the measurements of the resistivity is listed in Table 1. The measuring system IDAX 206 (and inbuilt software) was used to measure the loss factor tan (delta) using which the resistivity could be obtained. The frequency range was (0.01- 1000) Hz. The general trend observed throughout the measurements was that the measured resistivity increased with the decrease in frequency and below a certain frequency, it flattens out providing very low values. The conductivity at this frequency was defined as the DC conductivity. In the software, the capacitance of the cell is set as 23 pF if the cell IR1 was used for the resistivity measurement while in case of cell IR2, the capacitance value was changed to 22.67 pF.

3.2 Test cells for current measurements

3.2.1 CELL A

Figure 6 shows schematically the arrangement of the test cell A, which is the same cell that is used for the measurement of the resistivity IR2 [19]. It consists of an inner and outer electrode that is in the form of coaxial cylinder. The diameter of the inner electrode is about 43mm and that of the outer one is of 50.2 mm. The height of the test cell is 86mm. The gap between the electrodes is small (3.6 mm) and, hence, the field is almost homogenous. The cell is made of stainless steel and the lid has a BNC connector that can be used to directly connect the test cell to the electrometer for the measurement. The capacity of the test cell is 200 ml.

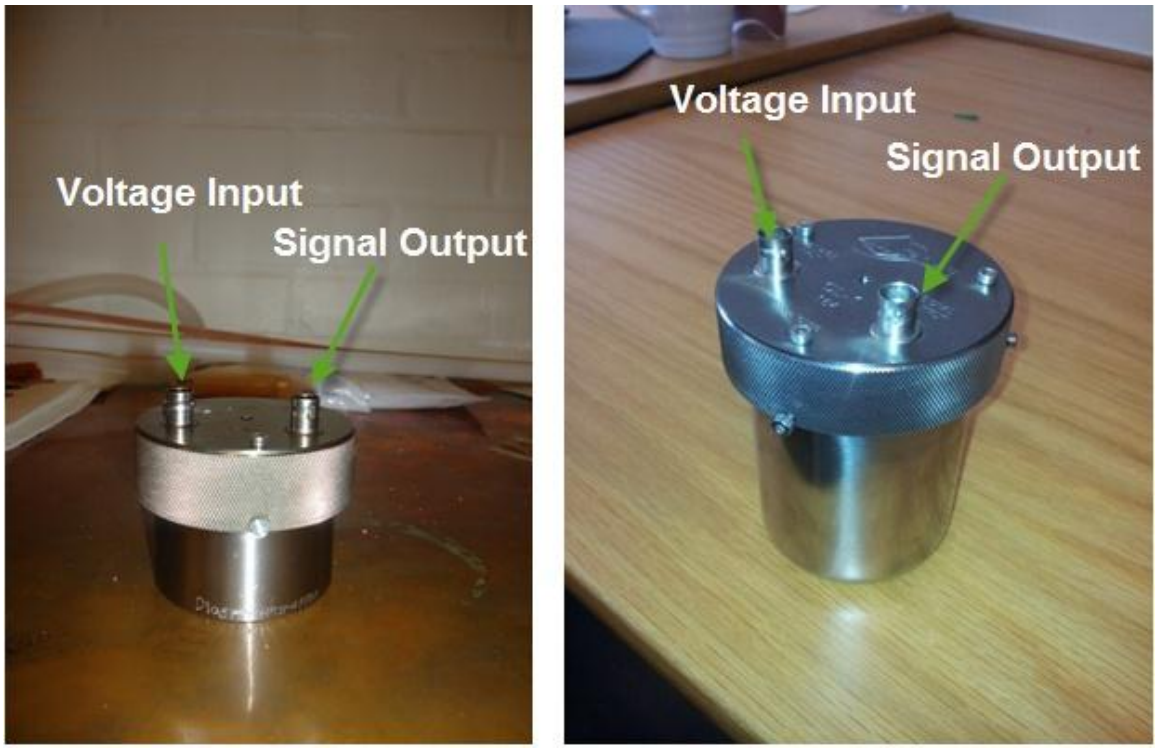

(a) (b)

Figure 5. IR1 (a) and IR2 (b) test cells [19] with the distance between cylindrical electrodes 1.5 mm and 3.6 mm respectively.

Table 1 Hardware used for the measurement of resistivity

Type	**Model**
Measurement system	IDAX 206[20]
Measurement cell	IR1, IR2 [19]

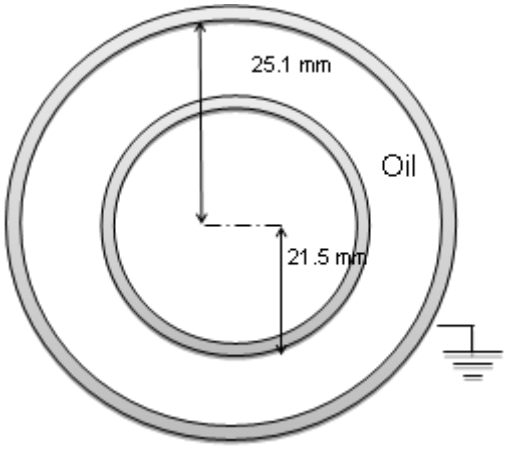

Figure 6. Electrode arrangement of test cell A (IR2).

3.2.2 CELL B

Figure 7 and 8 show the actual and schematic representation of test cell B which also looks like a coaxial cylindrical system. The inner electrode is 25 mm in diameter and the outer one is around 95 mm and the height is around 130 mm. The total capacity of the oil that can be filled in the cell is ~ 800ml. The electrodes are made up of polished stainless steel. The test cell is covered with a lid on top and bottom which is made of POM. The inner and outer electrodes are fixed tight with the help of viton rings which will prevent the oil from leaking out. The stainless steel outer electrode has 6 threads to fix the POM lid with the help of screws. The capacity of the test cell is ~600 ml.

Figure 7. The internal arrangement (a) and outer and general view (b) of cell B.

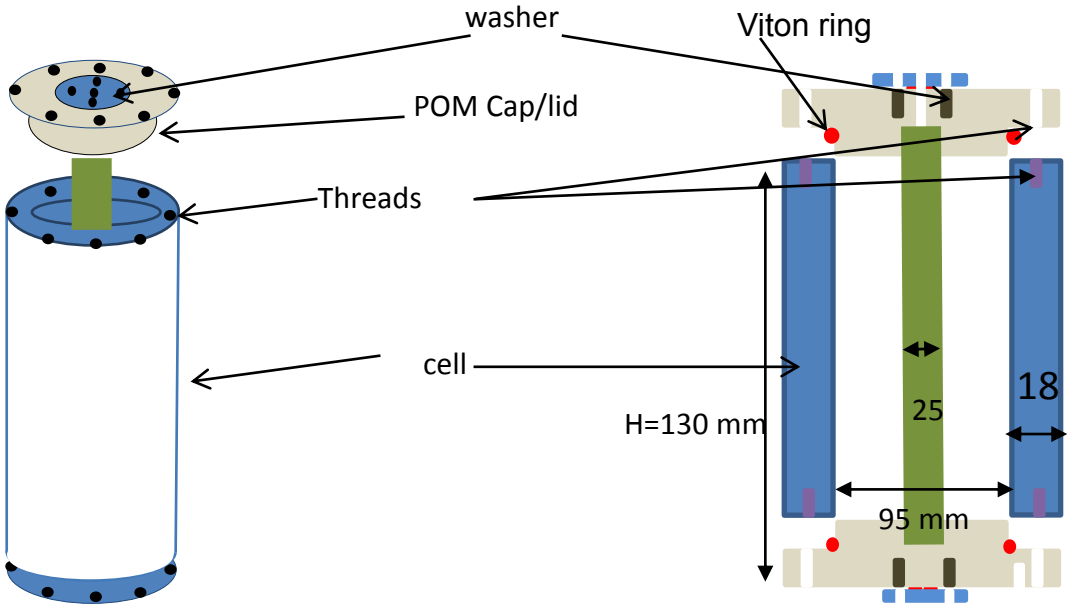

Figure 8. Schematic representation of the test cell B.

3.3 Connection set-up and Instruments used

The connection setup of the experiment is shown in Figure 9. The test cell shown in this figure is Test cell B. The test cell is to be connected to an electrometer KIETHLEY 6517 A which operates as both voltage source and current meter with a digital display. The electrometer is connected to the test cell with the help of a BNC cable connection. The inner electrode of the test cell is connected to the high voltage source terminal and the outer electrode is connected to the ground terminal of the electrometer, Figure 10. The entire set-up is placed in a grounded metallic bucket to reduce the noise level on the output signal, Figure 11. It was observed that the noise level or the pickup noise from the atmosphere decreased when the data was collected directly from the electrometer instead of transferring it to the oscilloscope or the data acquisition system. Hence the data is collected directly from the electrometer via General Purpose Interface Bus (GPIB) by using the LabVIEW software [21]. The collected data is plotted in the software called IGOR Pro [22].

All the test cells were separated by a protective cage from the rest of the devices and equipment for security issues. Opening the door of the cage would turn off the voltage source. The protective cage and the metallic bucket are connected to the common ground.

The connection set-up is similar to Test cell A but the only difference is that the Voltage Input terminal is connected to the High voltage source terminal and the Signal Output terminal is connected to the ground.

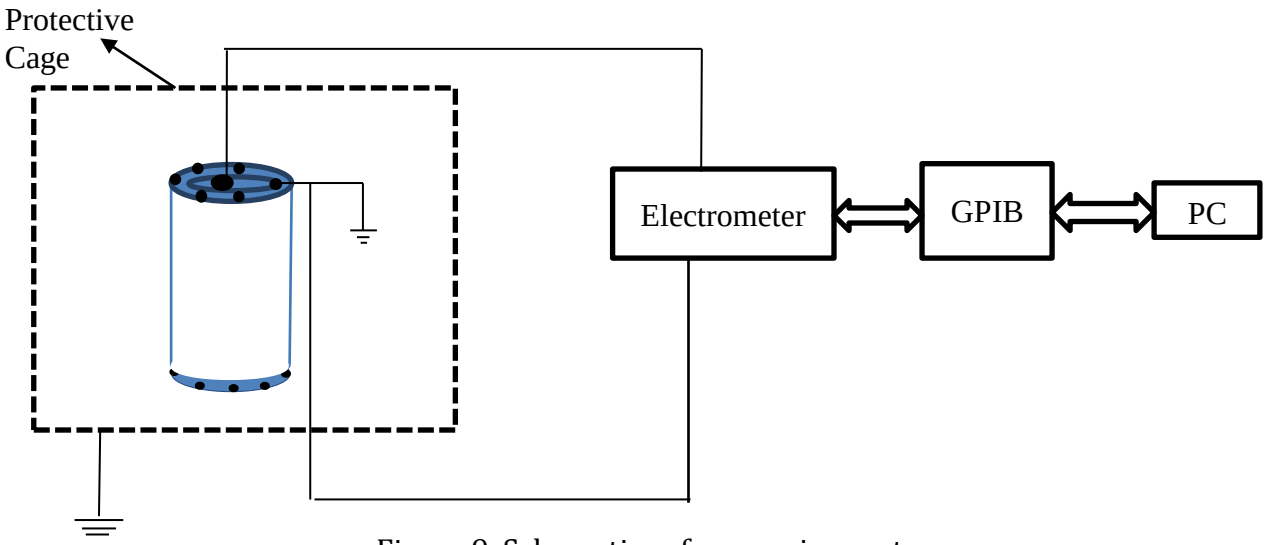

Figure 9. Schematics of measuring system.

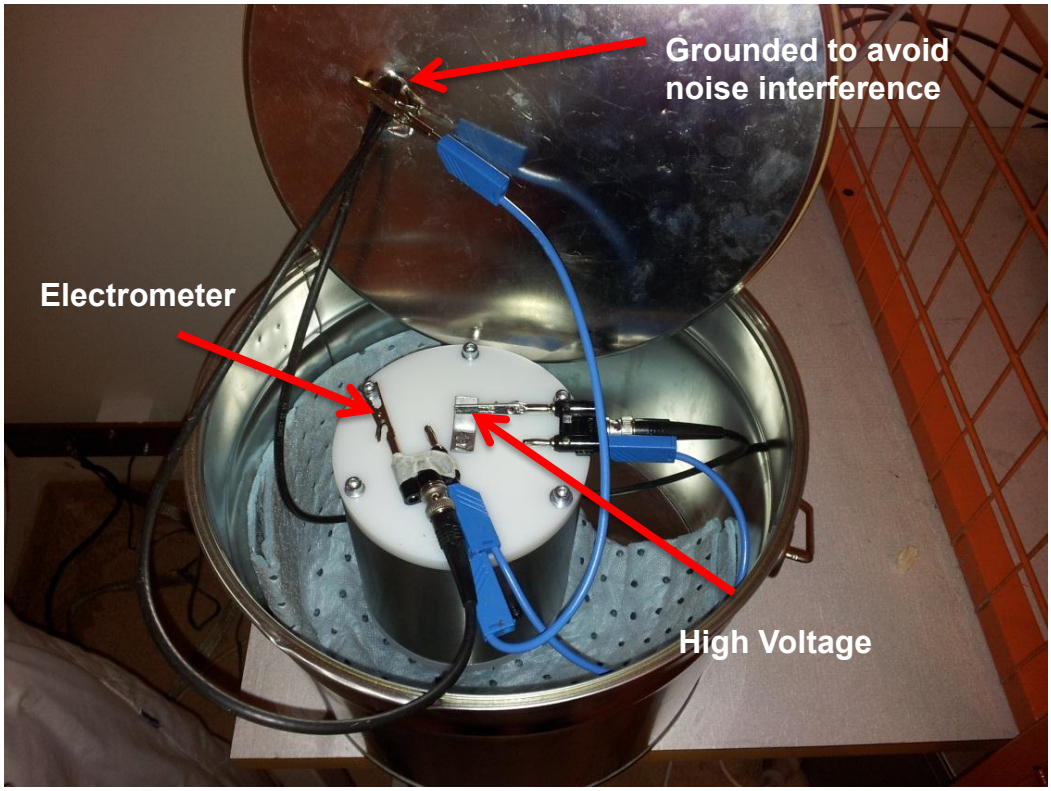

Figure 10. Connection diagram for the test cell B.

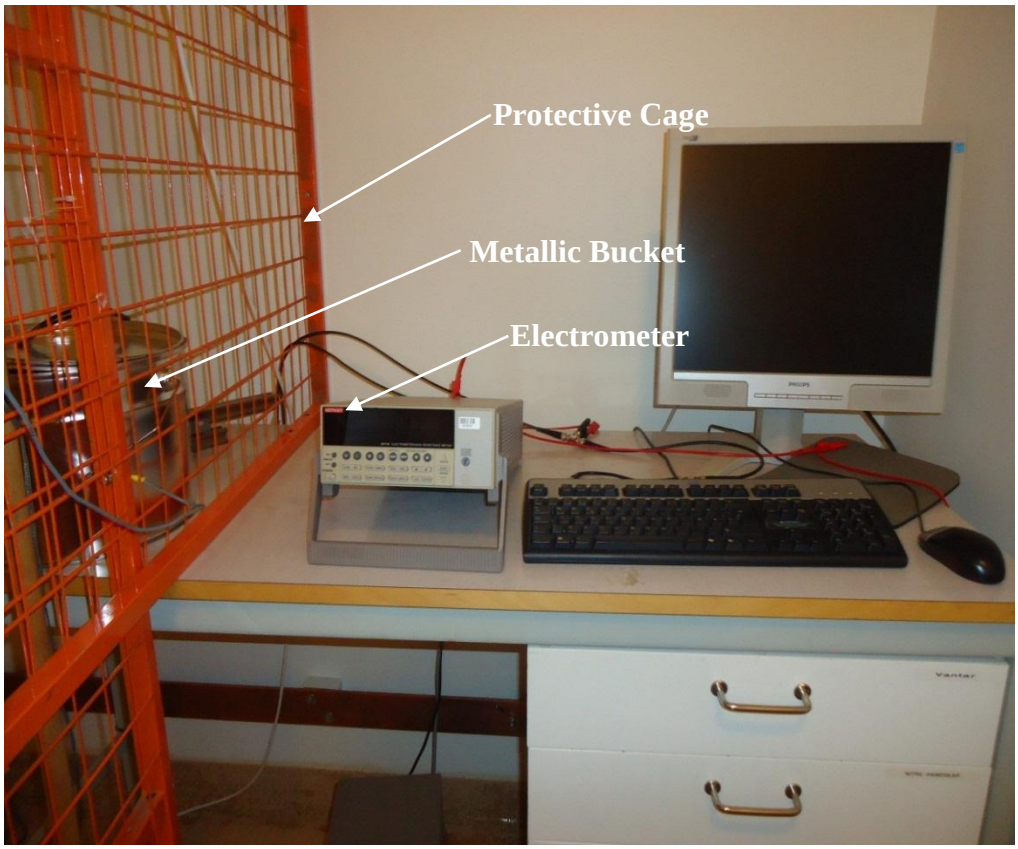

Figure 11. Test set-up used in the lab

3.4 Cleaning Procedures

3.4.1 Procedure 1

The parts of the test cell were disassembled. The cell was cleaned with warm water. It was washed with dish washing detergent and rinsed with water. Further, the cell was left to dry and then was washed with ethanol and rinsed with deionized water. After using ethanol, the cell was cleaned two-three times with cyclohexane and deionized water and was manually dried with paper to avoid the contaminations. Each part of the set-up was cleaned similarly and then reassembled. The cell was then filled with transformer oil from the barrel.

3.4.2 Procedure 2

The steps for this procedure were similar to procedure 1 but the major difference was that the cell was rinsed with transformer oil after washing it with cyclohexane and then filled with the oil from the barrel. The measurements of oil resistivity (presented below) showed that this procedure yielded the most stable results and, therefore, it was accepted as a standard procedure throughout the study.

3.4.3 Procedure 3

As mentioned earlier, the parts were washed with dish washing detergent liquid and ethanol. The primary difference here was that the cell was not rinsed with deionized water after cleaning it with ethanol. After cleaning with cyclohexane, it was then dried and filled with transformer oil.

4. RESULTS OF OIL RESITIVITY MEASUREMENTS

The oil that was used for the measurement is of the type Nitro- 10XN. After cleaning the cells according to the various procedures mentioned above, the resistivities of the barrel oil, oil from different test cells and oil with a drop of water were measured.

Figure 12 shows the resistivity of the oil from the barrel affected by different cleaning procedures. As it is seen, there is a prominent change in the value of resistivity for a lower frequency.

Figure 13 shows the resistivity the transformer oil from the different test cells after current measurements. It can be observed that the resistivity of the oil in test cell is much lower as compared to the oil from the barrel for different cleaning procedures.

From the figures it can be observed that there is a difference in the values of the resistivity for different cleaning procedures and different test cells. The change in the resistivity could be due to two major reasons: contaminations from the walls due to different cleaning procedure in the case of barrel oil and due to the presence of moisture from air in the case of different test cells as the vacant space and oil – air interface area is different for each cell. Since the resistivity is inversely proportional to the concentration and mobility of the ions, both factors may lead to their increase and corresponding reduction of the resistivity. To understand the sensitivity of the system to impurity/moisture, the same experiment was performed with the transformer oil containing a drop of water. After adding it to oil, the test cell was shaken to disperse the water. This did not change the resistivity of the oil much but addition of emulsions like TIAP or salt could make a drastic change in the resistivity [3]. The results of the test are shown in Figure 14 where it can be seen that the resistivity dropped drastically as compared to the clean oil.

The results of the resistivity measurement are summarized in Figure 15 and in Table 2. The values are given for the lowest frequency of 0.01 Hz. As shown, the resistivity of the oil changed for different types of the cleaning procedures. Hence based on the cleaning procedure and the resistivity, the oil could be classified into different types.

Barrel oil with cleaning Procedure 1

This oil was placed in the cell from the barrel that was cleaned according to procedure 1 with deionized water after cleaning it with ethanol. The resistivity of the oil with the cleaning procedure 1was measured as 3.3 1013Ω-m.

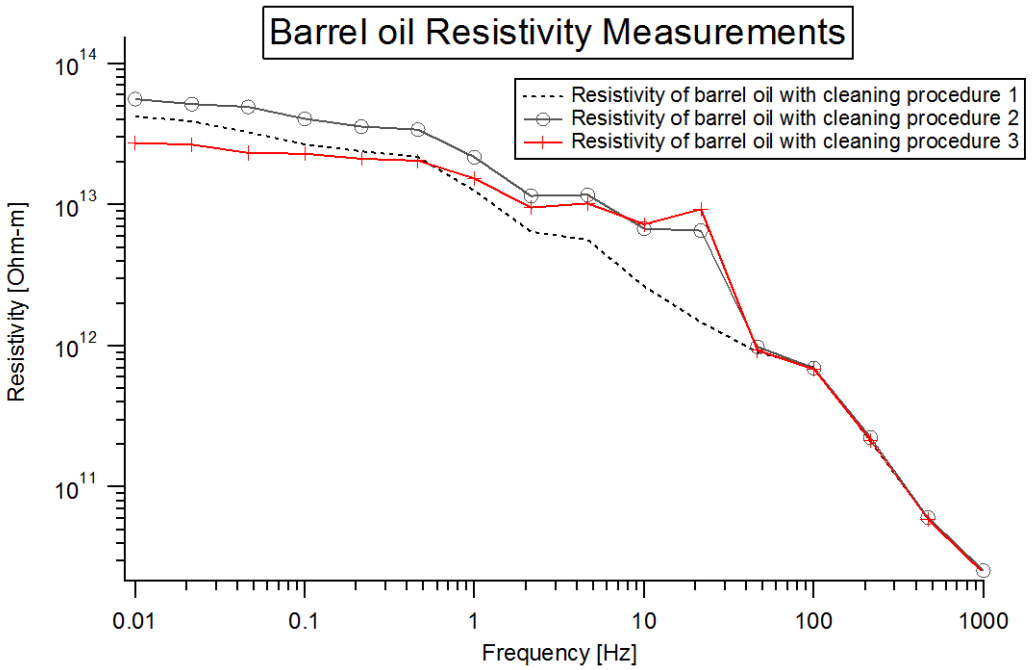

Figure 12. Resistivity of the transformer oil from the barrel for different cleaning procedures applied before the measurements

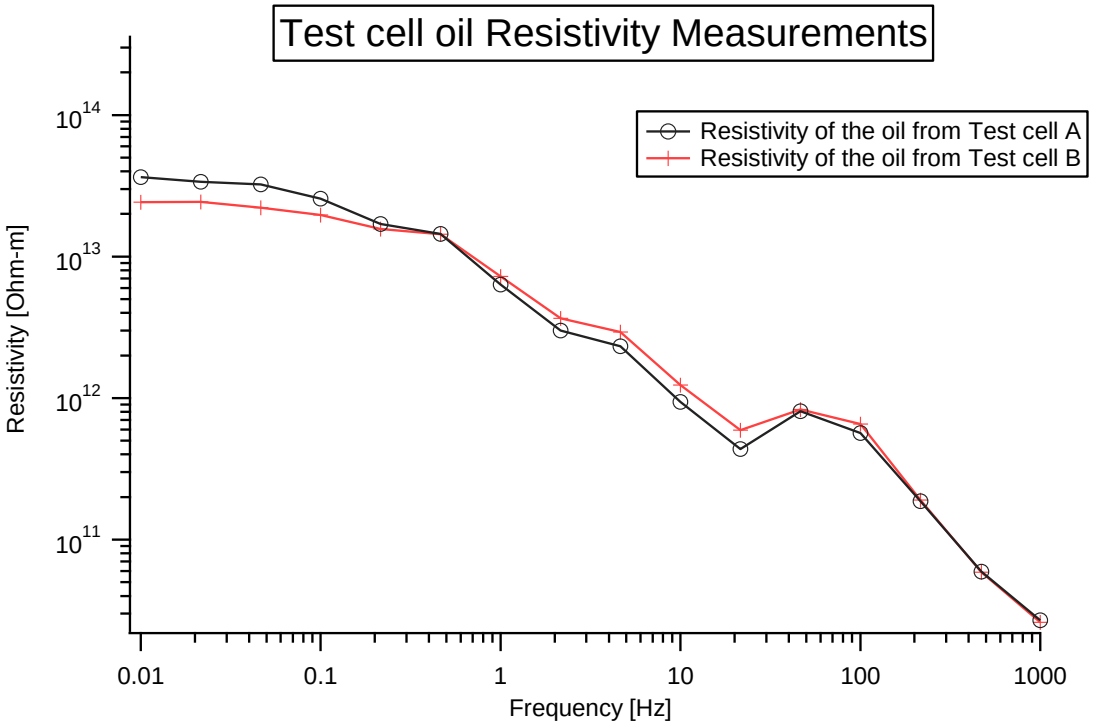

Figure 13. Resistivity of the transformer oil from different test cells after performing current measurements using cleaning procedure 2

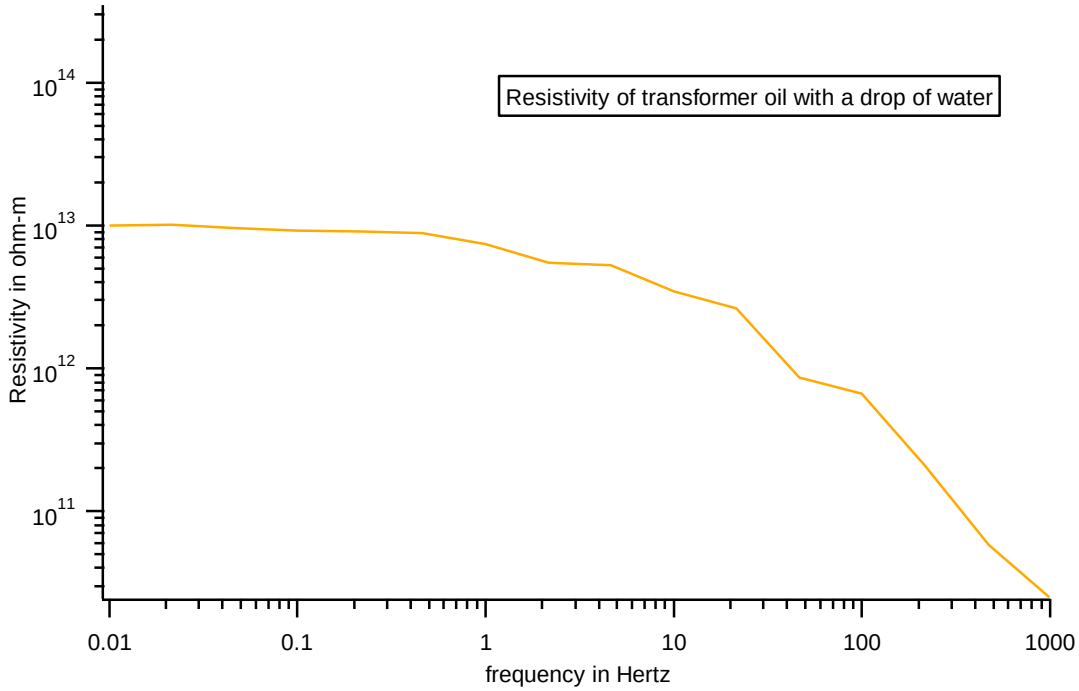

Figure 14. Resistivity of the transformer oil with a drop of water- it is a demonstration to illustrate the effect of humidity on resistivity of transformer oil

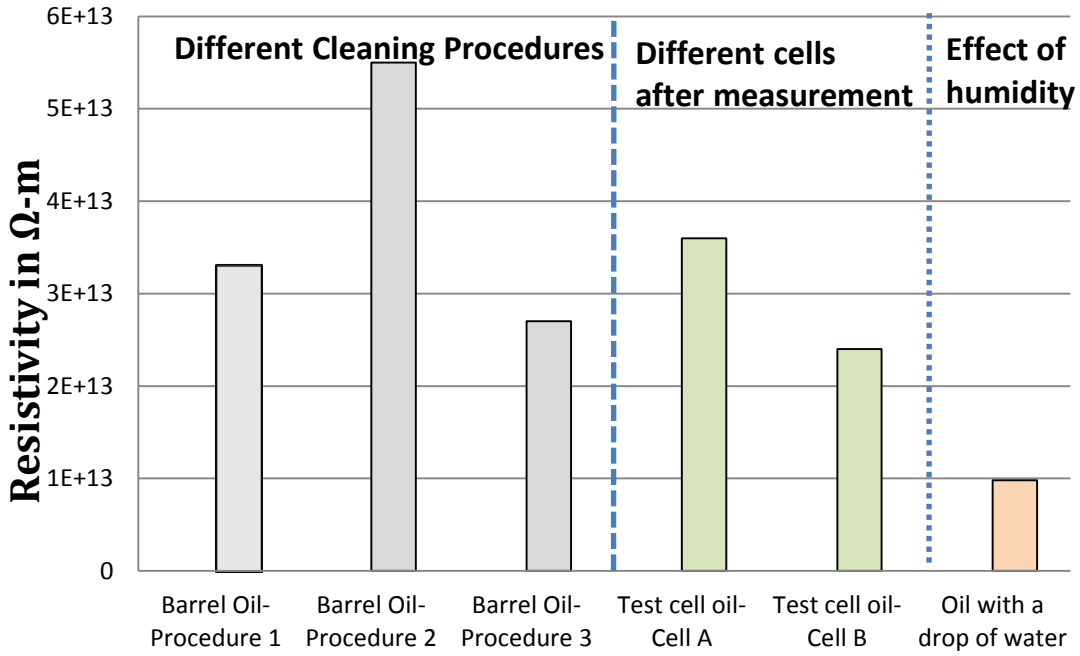

Figure 15. Resistivity of the transformer oil measured at frequency of 0.01 Hz.

Table 2 Oil Resistivity as shown in figure 15

Case	Resistivity, Ω-m
Barrel oil with Procedure 1	3.3 e^{13}
Barrel oil with Procedure 2	5.5 e^{13}
Barrel oil with Procedure 3	2.7e^{13}
Oil from Test cell A	3.6 e^{13}
Oil from Test cell B	2.4 e^{13}
Oil with a drop of water	9.8 e^{12}

Barrel oil with cleaning Procedure 2

This oil was placed in the cell from the barrel l that was cleaned according to procedure 2 with transformer oil after using cyclohexane. The resistivity of the oil from the barrel with the cleaning procedure 2 was measured as 5.55 1013Ω-m.

Barrel oil with cleaning Procedure 3

This oil was placed in the cell from the barrel that was cleaned according to procedure 3 without deionized water after using ethanol. The resistivity of the oil from the barrel with the cleaning procedure 3 was measured as 2.72 1013Ω-m..

Test cell A oil after measurements

This cell was cleaned according to procedure 2 and then filled with oil. After doing some experiments (Current measurements) in cell A, the resistivity of the oil from the test cell was measured as 3.6 1013Ω-m.

Test cell B oil after measurements

Similar to the previous case, this cell was cleaned according to procedure 2 and then filled with oil. After doing some experiments (Current measurements) in cell B, the resistivity of the oil from the test cell was measured as 2.4 1013Ω-m.

Oil with a drop of water

This is the oil with a lower resistivity because of the addition of a drop of impurity into the oil. For a cleaning mentioned above, the resistivity of the oil is found to be 9.4 1012Ω-m. But addition of a drop of water did not make the system have an inhomogeneous distribution.

5. IDENTIFICATION OF POLARITY OF ION INJECTION

This chapter begins with an analysis of transit and relaxation times of both the test cells. The main focus of this chapter is the experimental results obtained from single polarity and polarity reversal measurements for different test cells and different voltages to indicate the sign or polarity of ion injection.

First, to identify the typical time scales in the system, the transit and relaxation times for both the test cells were calculated using equations (18) and (19), respectively, and the results are shown in Figure 16. As discussed earlier, the transit time depends not only on the applied voltage and mobility but also on the dimensions of the inner and outer electrodes. Thus for an applied voltage of 400 V, the transit time for the test cell A was ~30 sec and for 1000 V for the test cell B, the transit time was ~1400 sec. The relaxation time depends on both the permittivity and the conductivity of the oil and it was calculated to be ~600 seconds.

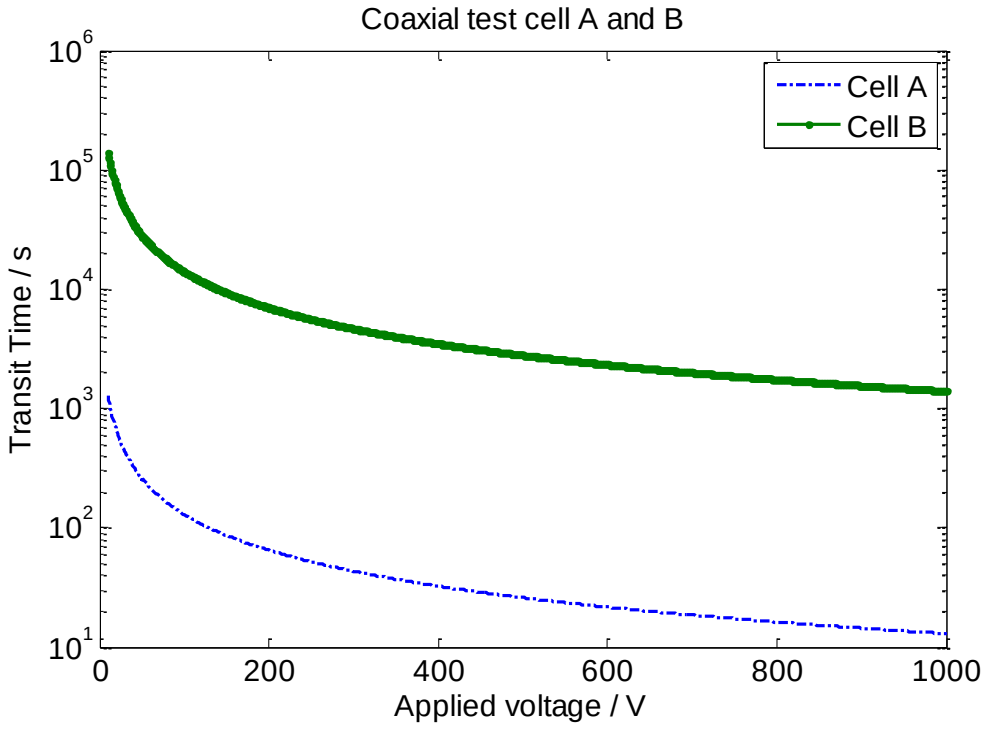

(a)

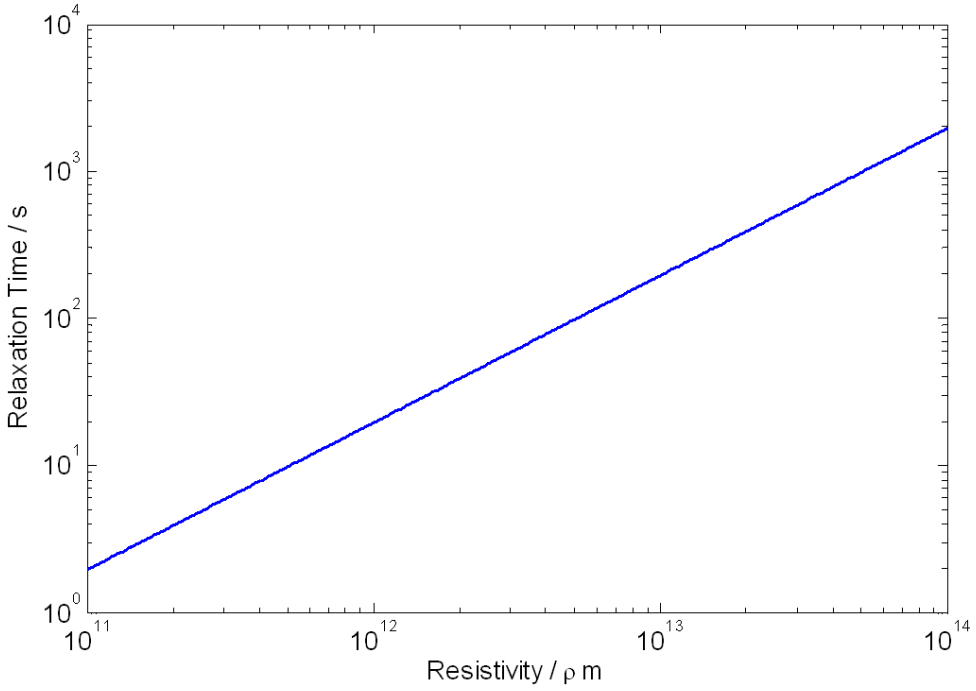

(b)

Figure 16. The calculated transit (a) and relaxation (b) times.

5.1 Results of current measurements with single polarity

When performing single polarity measurements for both test cells, the cells were grounded for 3 days. After that, a positive or a negative voltage was applied and the measurements were conducted. The reasons for the long grounding time are explained below in section 5.3.

Figure 17 shows the single polarity test results for cell A for the applied voltage of 400 V with oil resistivity 3.6·1013Ωm. In the plot, it can be seen that the steady state value of the positive current is higher than that of the negative current. There is also a 'shoulder' which appears at times that is in the order of the transit time. It can also be observed that the area below the positive current curve is much higher than that for negative current curve. The reason behind this phenomenon is not clear. One possible explanation could be due to certain physio-chemical reactions on the surface of the electrode. It must also be noted that the current does not reach its steady state value whereas it keeps decaying throughout.

The results of the measurements with cell A at the applied voltage of 1000 V and oil resistivity 2.4·1013Ω-m (obtained after performing the current measurements) are shown in Figure 18.

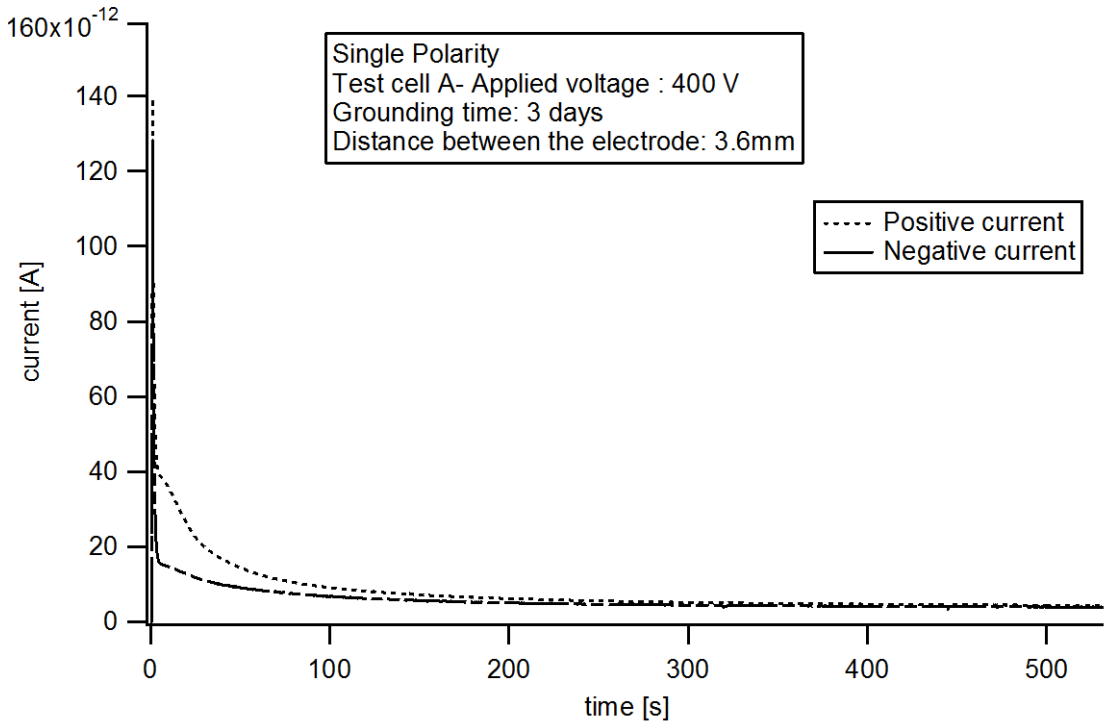

Figure 17. Current measured in the test cell A at 400 V.

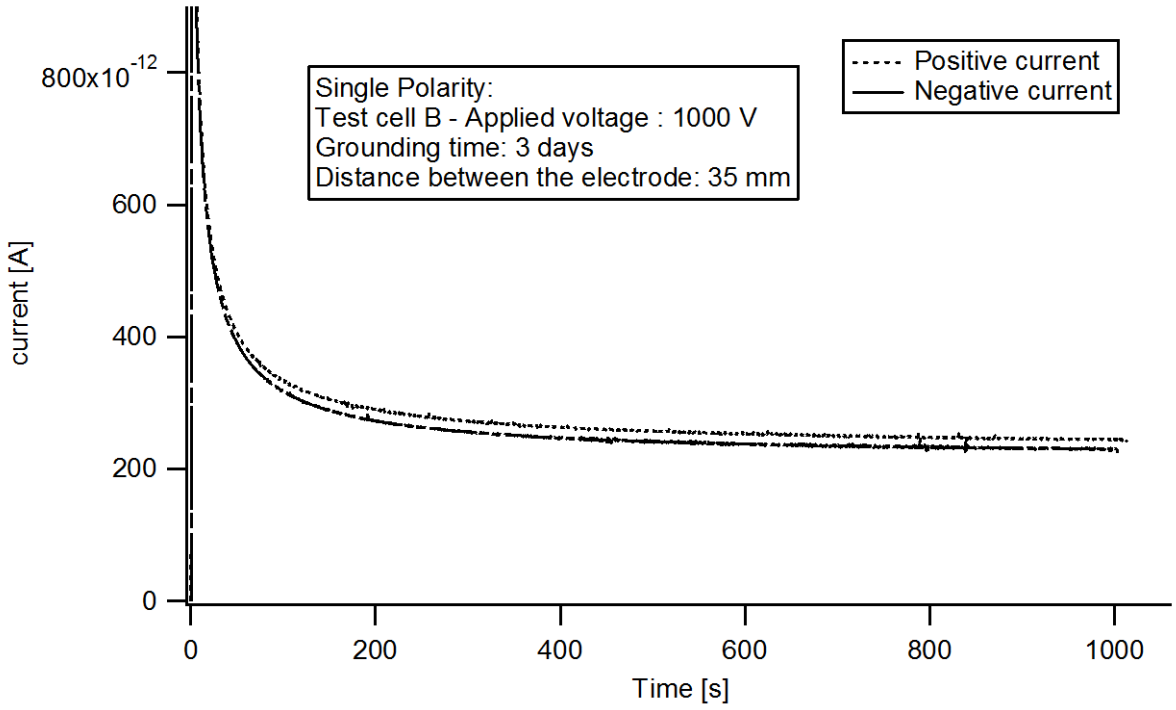

Figure 18. Results of single polarity current measurements for the applied voltage of 1000V to test cell B.

It can be seen that, at the time of application of the test voltage, the magnitudes of the currents at different polarities are almost the same but there is a slight difference in the steady state values: the positive current is higher in magnitude when compared to the negative one. The currents keep decaying even after 1000 s and do not approach a steady state value. However after a certain time, the decay is

very slow and, hence, the corresponding value can be assumed to be close to the steady state values.

5.2 Results of current measurements with polarity reversal

In case of test cell A, after performing the single polarity measurements at positive applied voltage +Ua for 600 s, the polarity on the inner electrode was reversed to -Ua. The resulted current was measured for 600 s and then the polarity was reversed again to +Ua. This was done for different magnitudes of the test voltage. But due to pick up noise, it was observed that the higher voltages are more relevant when compared to lower voltages. Hence, the experiment was performed twice to for the applied voltage of Ua= 400 V to check reproducibility of the results.

Figure 19 shows results obtained for cell A for an applied voltage of 400 V after performing single polarity measurement.

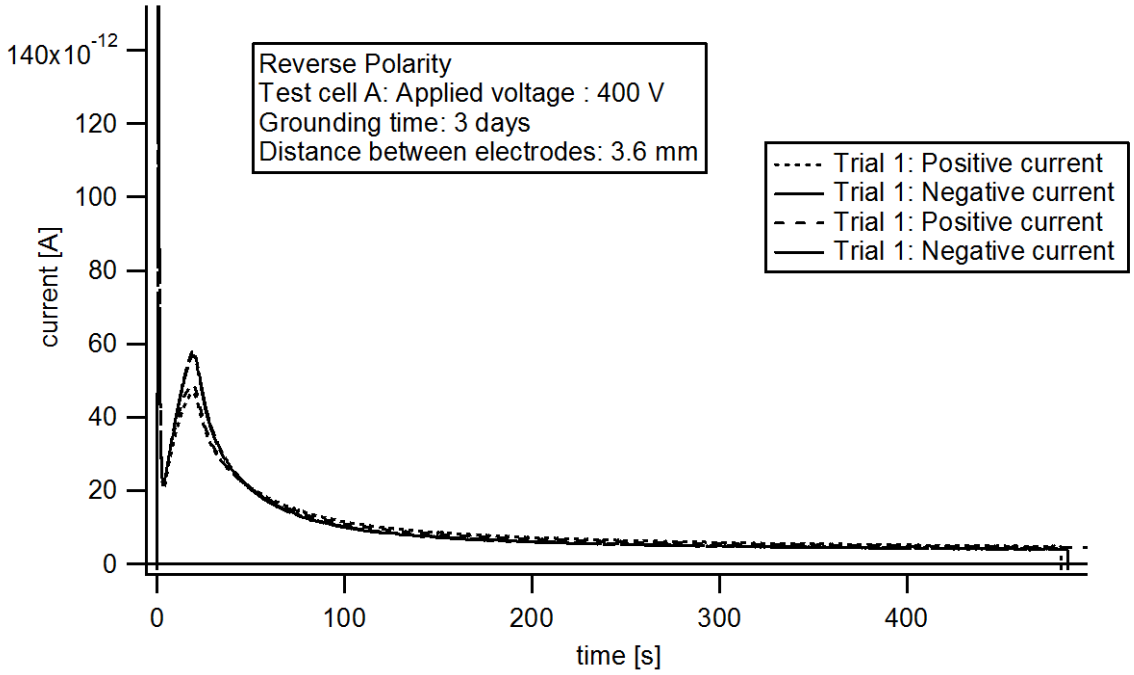

Figure 19. Polarity reversal current measurement for the applied voltage of 400 V to test cell A.

From the plot, it can be observed that, at the time of polarity reversal, the magnitude of the negative current is higher than the magnitude of the positive current. After a certain time, the current seems to decay rapidly. After the transit time, there is a change in the slopes of the positive and the negative currents and both the curves crossover each other. After this point, it is seen that the positive current is higher than the negative current. It can be clearly seen that the area under the peak for the negative current is lesser than that for the positive current.

This method was also used for the case when a single polarity measurement at -400 V was conducted first and then reversing the polarity to +400 V and then to -400 V again was performed. This test yielded similar results as shown above.

In case of test cell B, after performing the single polarity measurement at +1000 V for 1000 s, the polarity on the inner electrode was reversed to -1000 V. This current was measured for 1000 seconds and then the polarity was reversed again to +1000 s.

Figure 20 shows the polarity reversal case for cell B for an applied voltage of 1000 V after performing single polarity measurement. From the plot, it can be observed that, at the time of polarity reversal, the magnitude of the negative current is higher than the magnitude of the positive current. It can be seen that there is difference between the positive and negative current for certain time at the beginning of the curve.

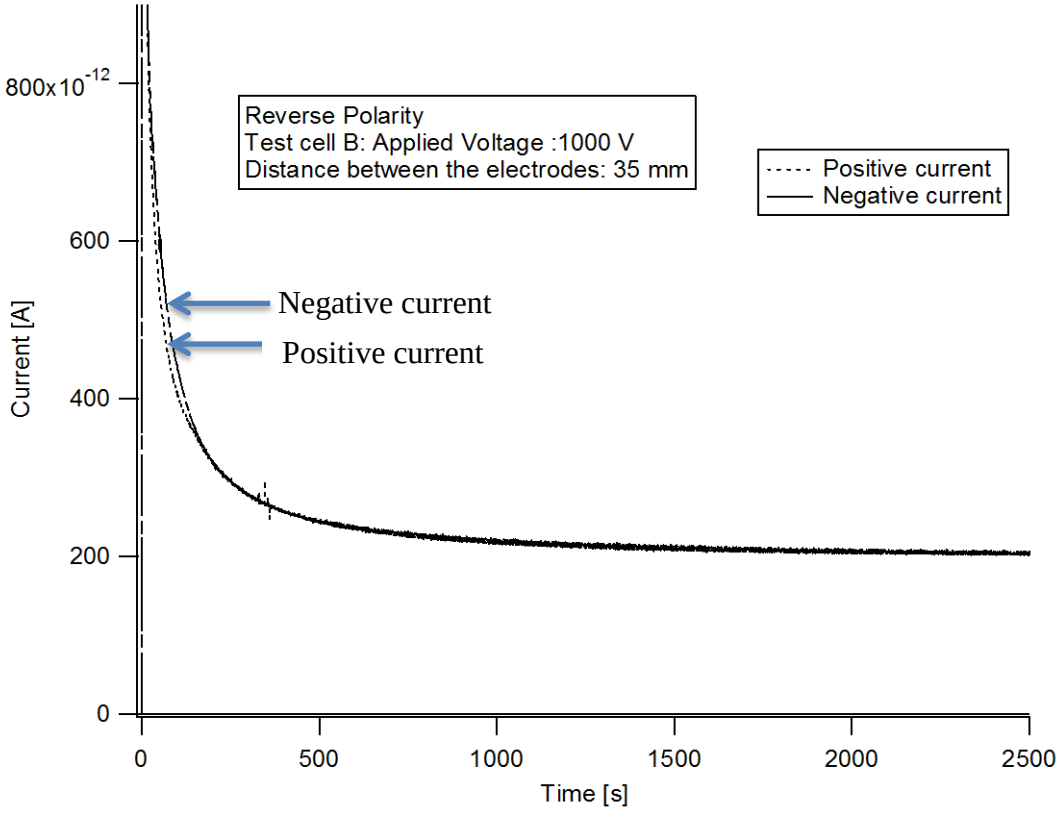

Figure 20. Current after polarity reversal of voltage 1000 V applied to test cell B.

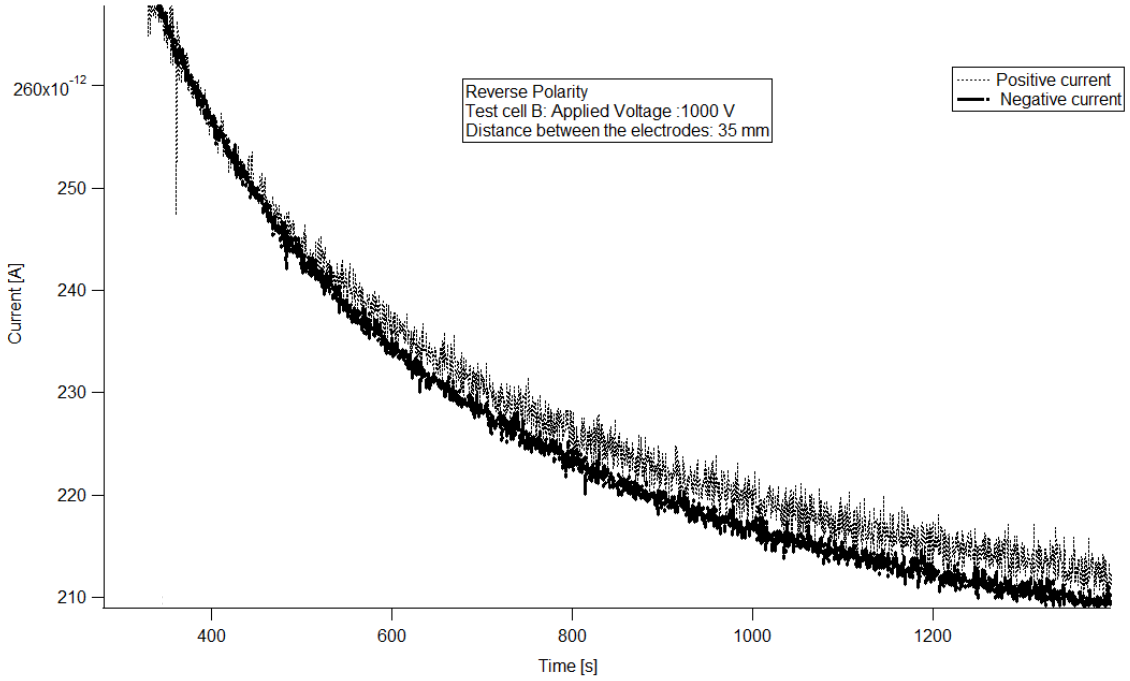

Figure 21. Polarity reversal current in cell B at 1000 V. Zoomed in plot of fig. 20

After a certain time, the current seems to decay rapidly. After sometime, there is a change in slope between the positive and the negative current and both the curves crossover each other. After this point, it is seen that the positive current is higher than the negative current. It can be clearly seen that the difference between the steady state current for positive and negative current in case of single polarity is higher than the difference between the steady state current for positive and negative current in the case of polarity reversal. The difference in the values of steady state current is shown in table 3 in chapter 6.

5.3 Effect of grounding time

During the experiments, it was noticed that the shape and the slopes of the current curves for single polarity measurements were different and not reproduce-able. It was observed that the current curves depended on the time the system was turned off and grounded that could be related to the time needed for the ions that were buildup on the surface of the electrode to reach equilibrium. To clarify this effect, the current measurements were performed for both polarities by grounding the system prior the experiments for different time intervals from minutes to days.

Figure 22 and Figure 23 show the results of single polarity measurements for different grounding times for positive and negative currents, respectively, for cell A. From the figures, it can be clearly seen that for shorter grounding time, there is a buildup of charges that could possibly cause a peak in the current when the layer of ions reaches the opposite electrode when the polarity is switched. Hence the minimum time for the system to attain a state of equilibrium would be in the order of days. Hence the system was grounded for 3 days before performing single polarity measurements.

The results obtained with the test cell B are slightly different. As it is seen in Figures 24 and 25, there is no 'bump' in the current traces in case of test cell B when compared with the test cell A. One reason could be due to the presence of bulk liquid in case of the test cell B and thus the field is more inhomogeneous than the test cell A and the ratio between the surface and the bulk is different for both the test cells which may also be one of the possible reasons for a 'bump' in the current measurements.

Based on the presented results, it was decided that the system has to be grounded for 3 days before performing single polarity measurements and the results shown above in sections 5.1 and 5.2 correspond to this case.

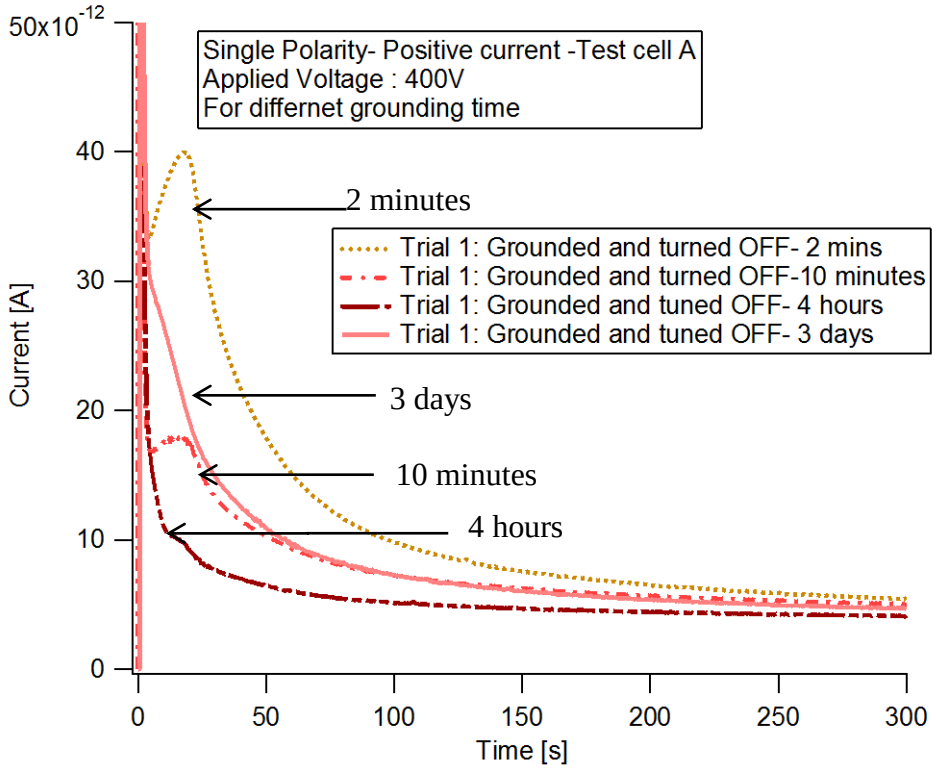

Figure 22. Single polarity positive current measurement at 400 V applied to cell A.

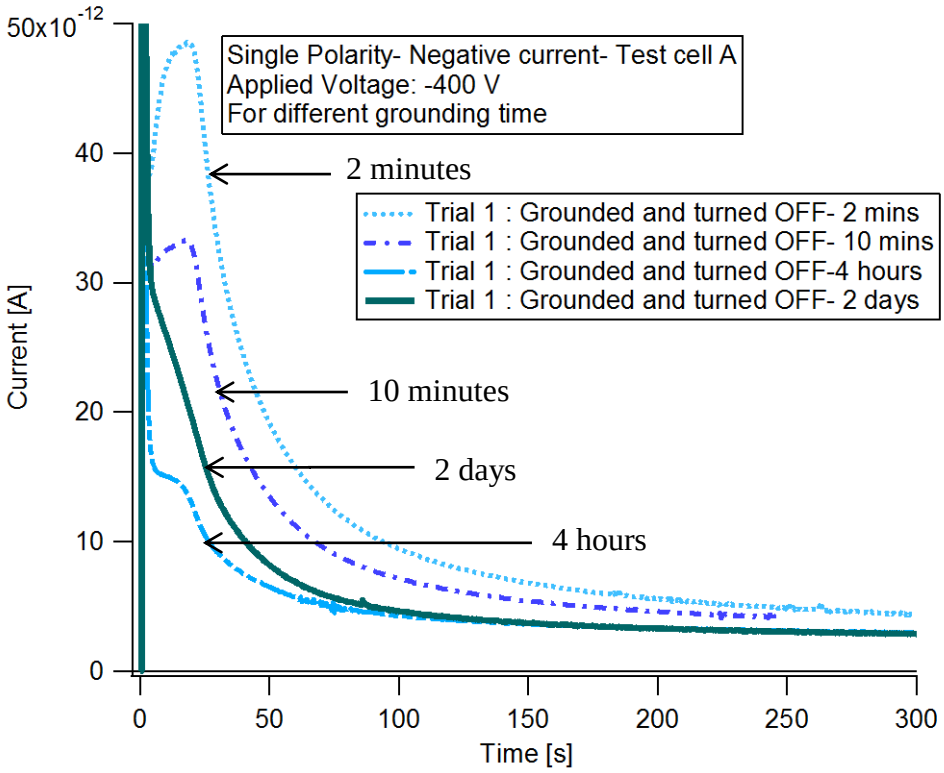

Figure 23. Single polarity negative current measurement at 400 V applied to cell A.

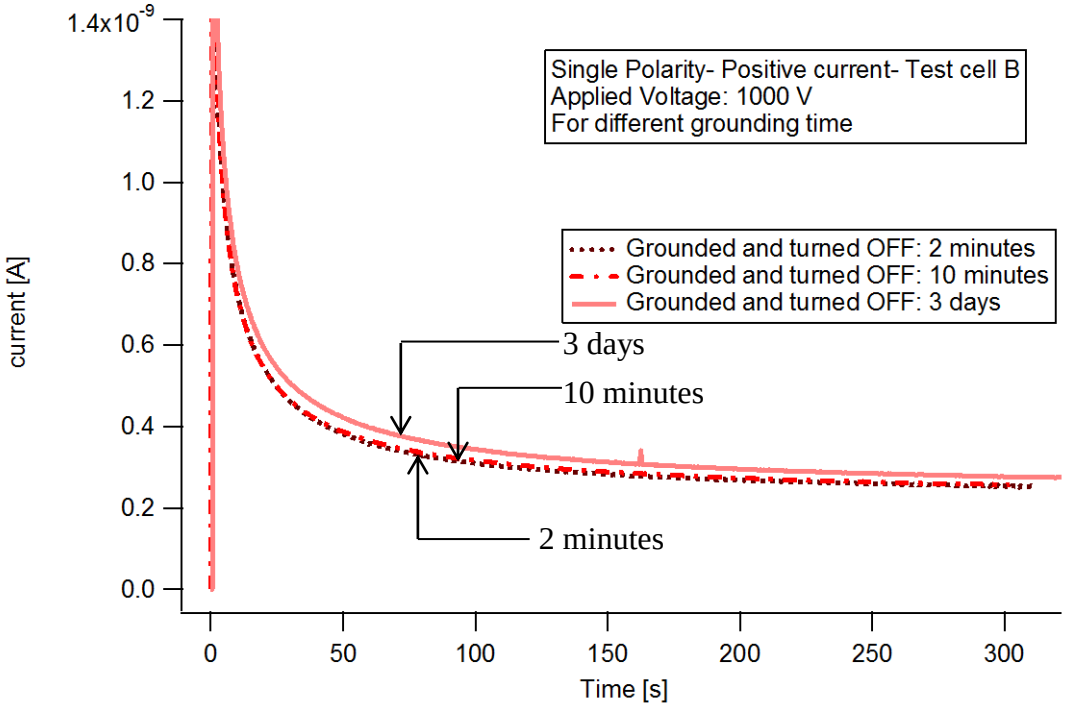

Figure 24. Single polarity positive current measurement at 1000 V applied to cell B.

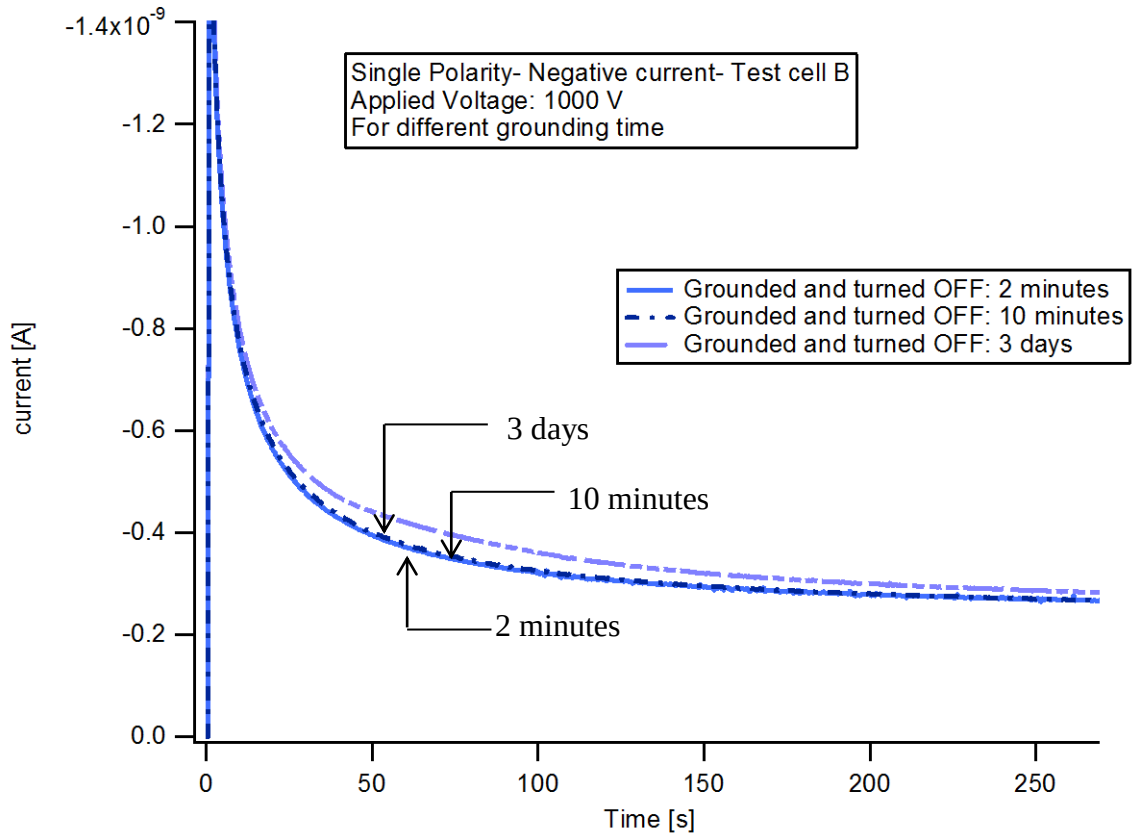

Figure 25. Single polarity negative current measurement at 1000 V applied to cell B.

6. DISCUSSION

From the results of single polarity and polarity reversal methods, the three main observations were (a) polarity dependence of injection (b) charge carrier movement at polarity reversal and (c) time aspects of grounding.

(a) Polarity dependence of injection

The steady state current measured with the test cell A using both the single and polarity reversal methods are shown in figure 26. The variation of the experimental data was found to be as small as ± 0.03·10-12 A which was due to the pickup noise from the surrounding. It is to be noted that the current was decaying and never attained a steady state value. But the decaying rate of the current was very slow after approximately 450 seconds and hence the steady state current for the test cell A was taken at 475 seconds for both the polarities (positive and negative) currents and both the measurement techniques (single and polarity reversal). The applied voltage for this test cell was 400 V.

Similarly figure 27 shows the comparison of the steady state current for the test cell B. The variation of the experimental data was found to be ± 0.01·10-10 A which was due to the pickup noise from the surrounding. It is similar to the case of test cell A where the current was decaying and never attained a steady state value. But the decaying rate of the current was very slow after approximately 900 seconds and hence the steady state current for the test cell B was taken at 1000 seconds for both polarities and for both the measurement techniques. The applied voltage for this test cell was 1000 V.

It can be seen from the figures, the values of the positive steady state current are higher than that of the negative one for both the techniques. Note that the total steady state current is the sum of the source current and the displacement current. The current measured in cell B are higher than those in cell A. This is related to the fact that the field inhomogeneity is stronger in cell B and more ions can be injected into the oil due to stronger field at the inner electrode.

Table 3 summarizes the steady state values obtained with both the test cells according to the figure 26 and figure 27.

It can be clearly observed that the magnitude of the positive steady state current is always higher than that of the negative one in different geometries and also for different measurement techniques. The difference between positive and negative steady state current in cell A are higher for the reverse polarity method whereas, in case of test cell B, the difference is higher for the single polarity method. This indicates clearly that the sign of ion injection is positive.

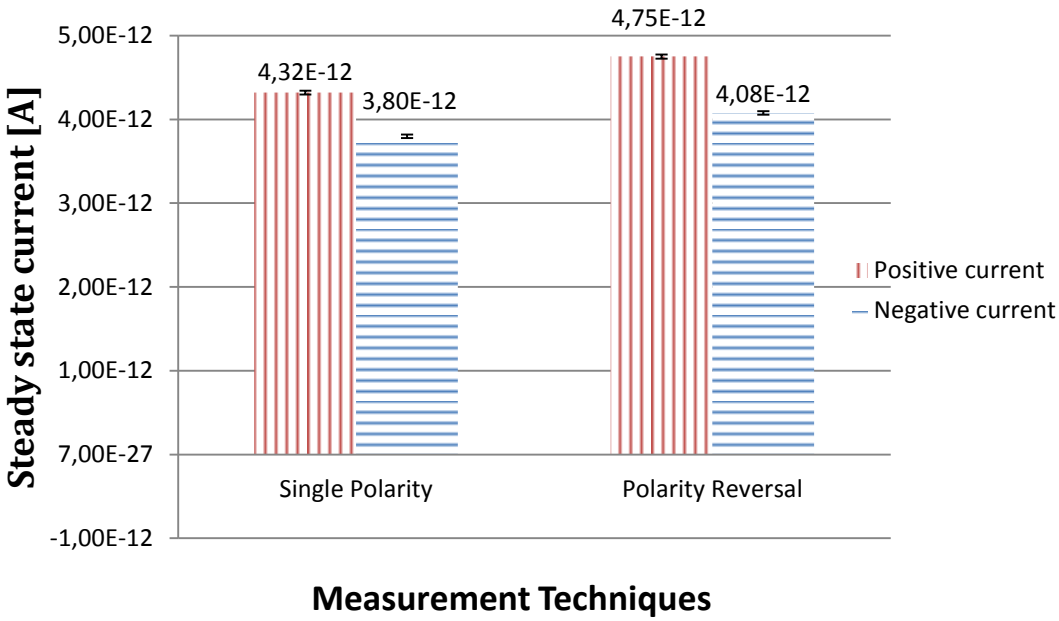

Figure 26. Comparison of the positive and negative steady state currents for both measurement techniques at t = 475 s for the voltage of 400 V applied to cell A.

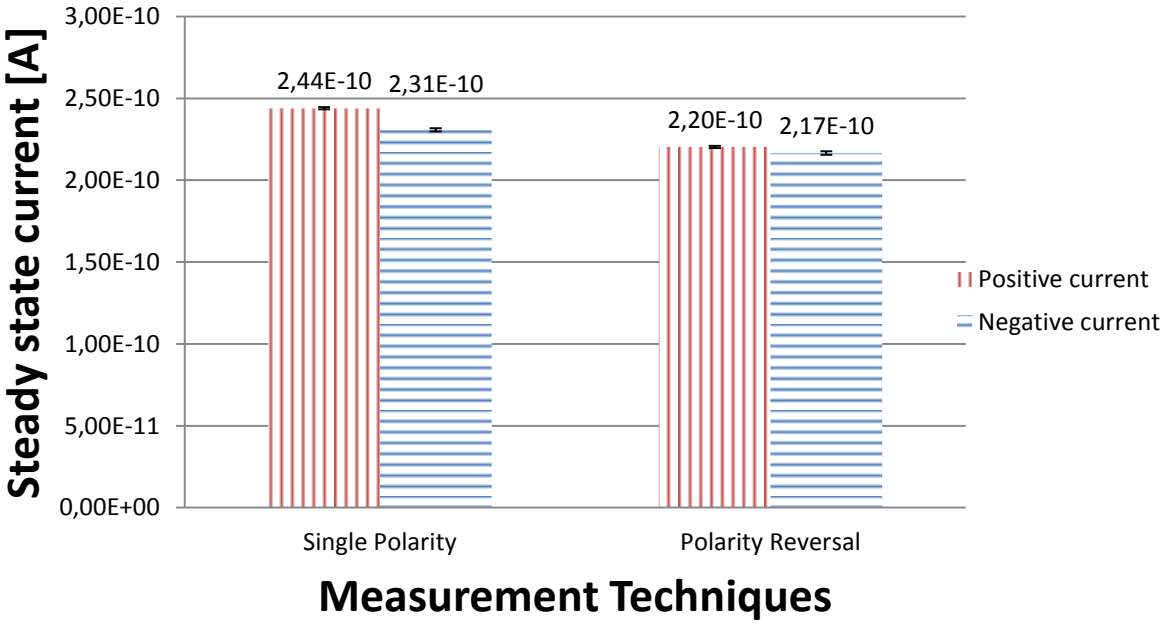

Figure 27. Comparison of the positive and negative steady state currents for both measurement techniques at t = 1000 s for the voltage of 1000 V applied to cell B.

Table 3. Steady state current values and the differences between them for different techniques

Cell A	Single Polarity Method	Polarity Reversal Method
Positive current [A]	(4.32±0.024)E-12	(4.75 ±0.024)E-12
Negative current [A]	(3.80±0.024)E-12	(4.08 ±0.024)E-12
Difference [A]	(0.52±0.024)E-12	(0.67±0.024)E-12
Difference in percent	13 %	15 %

Cell B	Single Polarity Method	Polarity Reversal Method
Positive current [A]	(2.44±0.01)E-10	(2.20±0.01)E-10
Negative current [A]	(2.31±0.01)E-10	(2.17±0.01)E-10
Difference[A]	(0.13±0.01)E-10	(0.03±0.01)E-10
Difference in percent	5%	1%

Figure 28 shows the comparison between the experimental and simulation results of test cell A single polarity current measurement. The simulations were performed based on a model presented in chapter 2 and are described in details in [11]. The figure illustrates that by changing the level of injection in oil with fixed resistivity 3·1013 Ωm, the steady state current can be changed. Thus increasing the level of injection for the given resistivity will also increase the steady state current drastically and decreasing the level of injection would decrease the magnitude of the current. By changing the levels of injection with respect to the steady state current, the best fit for the right experimental and simulation steady state current can be obtained.

It was also observed in the simulation that the change in the oil resistivity at a fixed level of injection leads to variations of the current at the initial stage. It gives rise to a current curve which is similar (has a 'shoulder') to the one obtained from the experimental results. The simulations for this case are shown in the appendix. This effect is also illustrated in Figure 29 where the comparison between the experimental and simulation results for the test cell B at single polarity is shown. One can observe in the figure that by changing the oil resistivity for a fixed level of injection, the steady state current can be changed. Thus, increasing the oil resistivity will decrease the steady state current drastically and decreasing the resistivity for a given level of injection would increase the magnitude of the current. Note that in this case the level of injection is set in the simulations to 0.1 for different resistivity for an applied voltage of 1000 V.

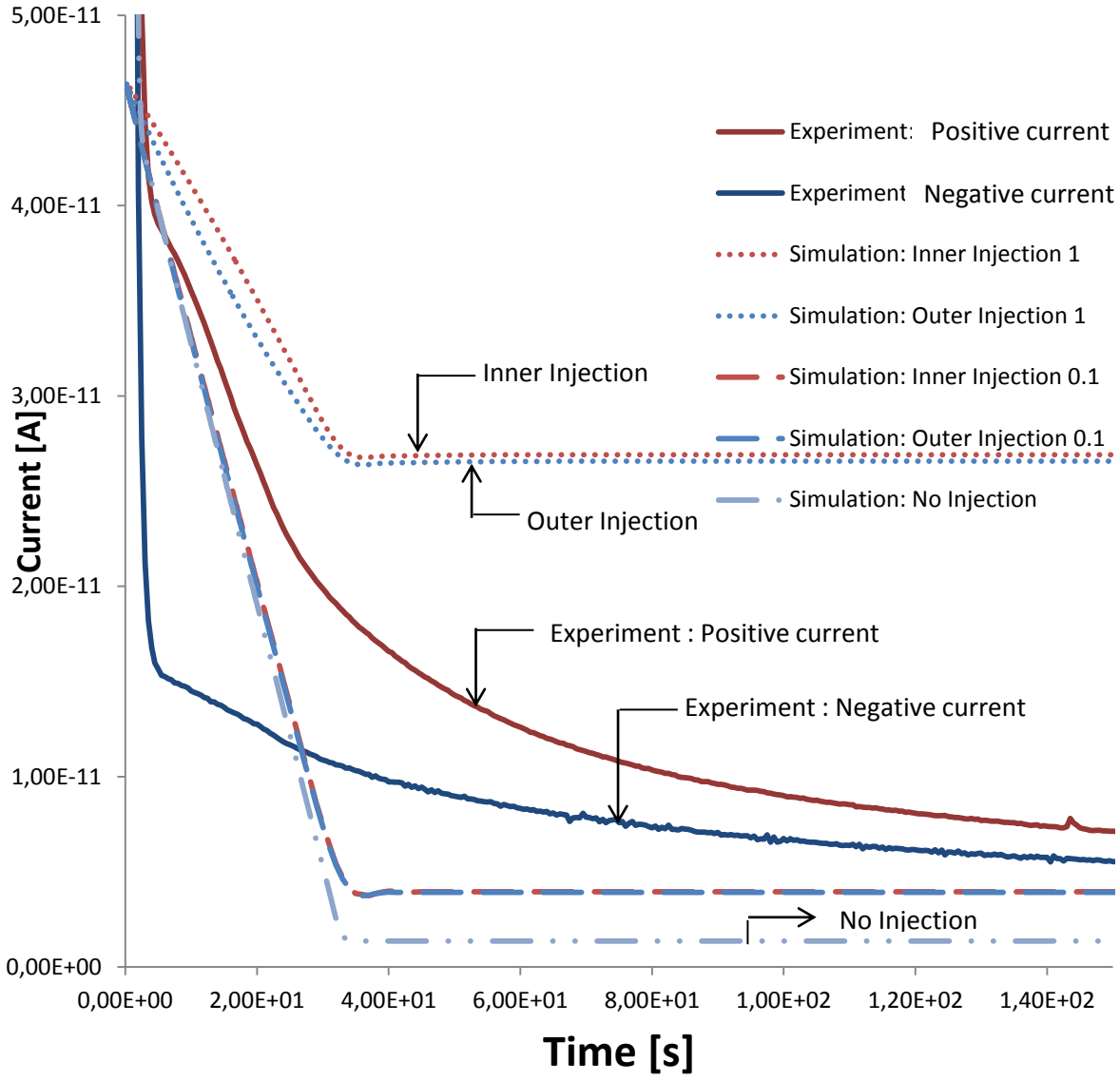

Figure 28. Comparison between the experimental and simulation current measurement for single polarity method for test cell A at 400 V for different levels of injection.

(b) Charge carrier movement during polarity reversal

It was observed in the experiments that the polarity reversal method applied with the test cell A always provided a peak current at instants which were in the order of the transit time. The reason for this effect is not clear yet. It is believed that one of the explanations could be related to the polarity dependent pile up of charges on the surface of the electrode. The experimental and simulation plots for the polarity reversal for test cell A for the applied voltage of 400 V are shown in figure 30.

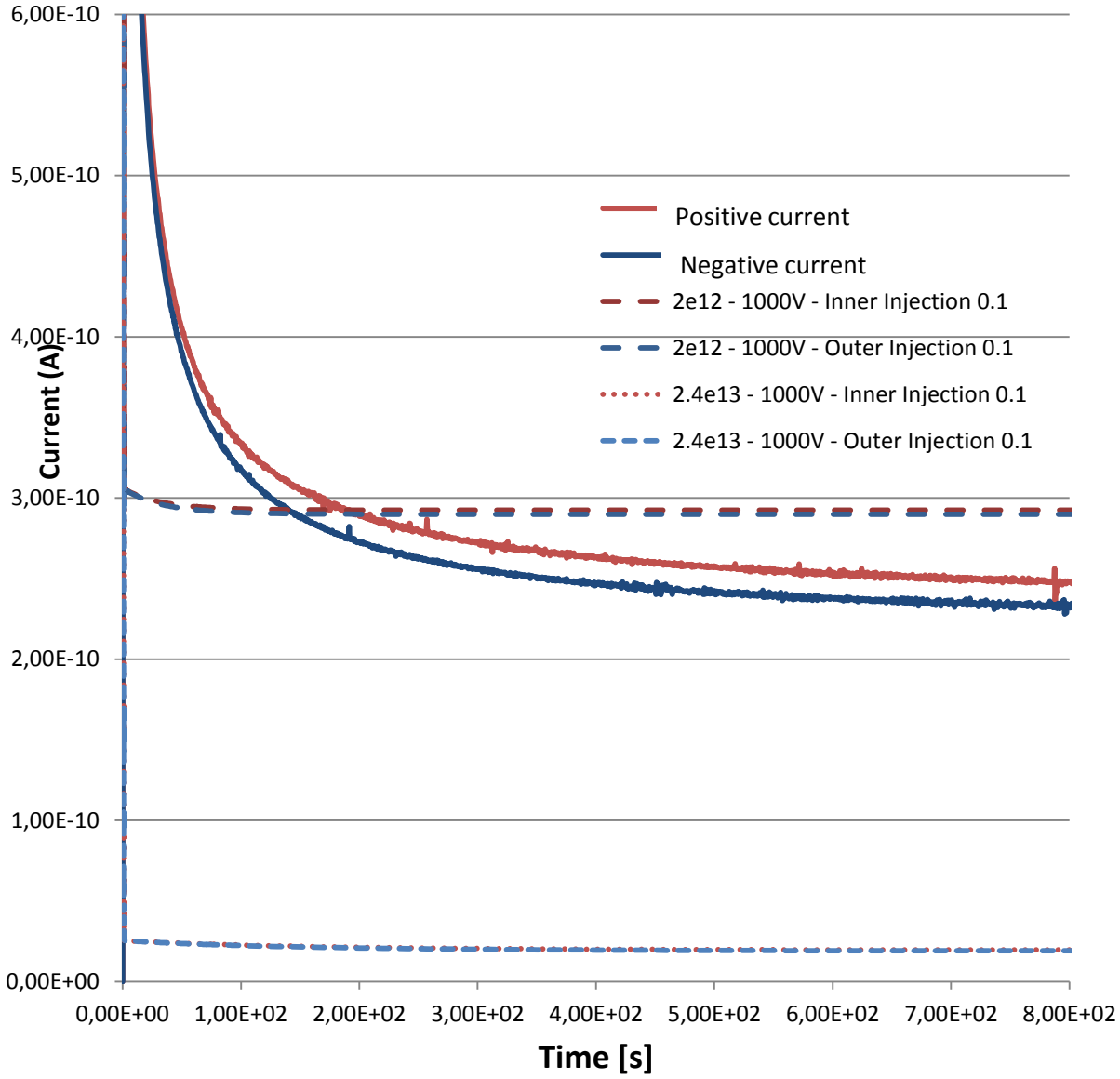

Figure 29. Comparison between the experimental and simulation current for single polarity method for test cell B at different resistivity.

As it is seen, the differences in the measured currents are much higher than that obtained from the simulations. Actually, the latter can be recognized only in the zoomed plot in Figure 30b. This indicates that there are some additional processes taking place in the real system that are not being considered in the model presented in chapter 2. However, it was noticed in the simulations that changing the level of injection for the results from Figure 30 (a) leads to a rise of the difference between the currents of different polarity and provides a current curve which is similar to that (with the 'bump') obtained from the experiments. The simulations for this case are given in the appendix.

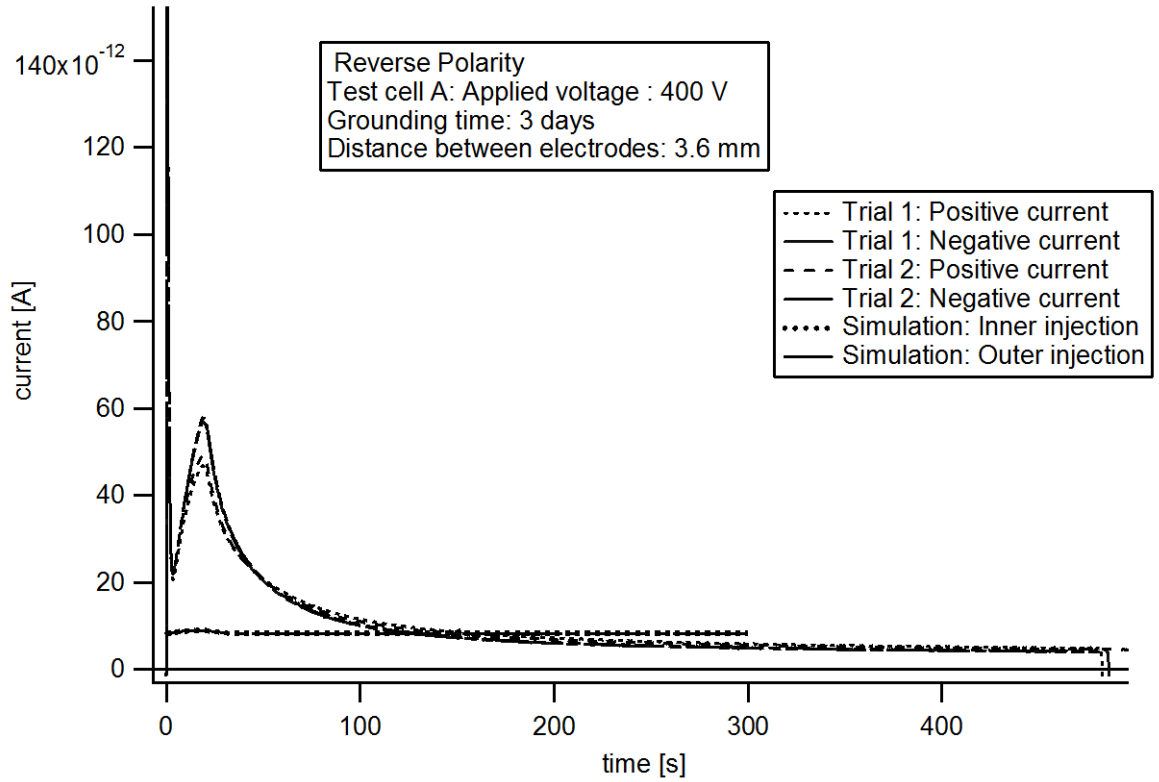

(a)

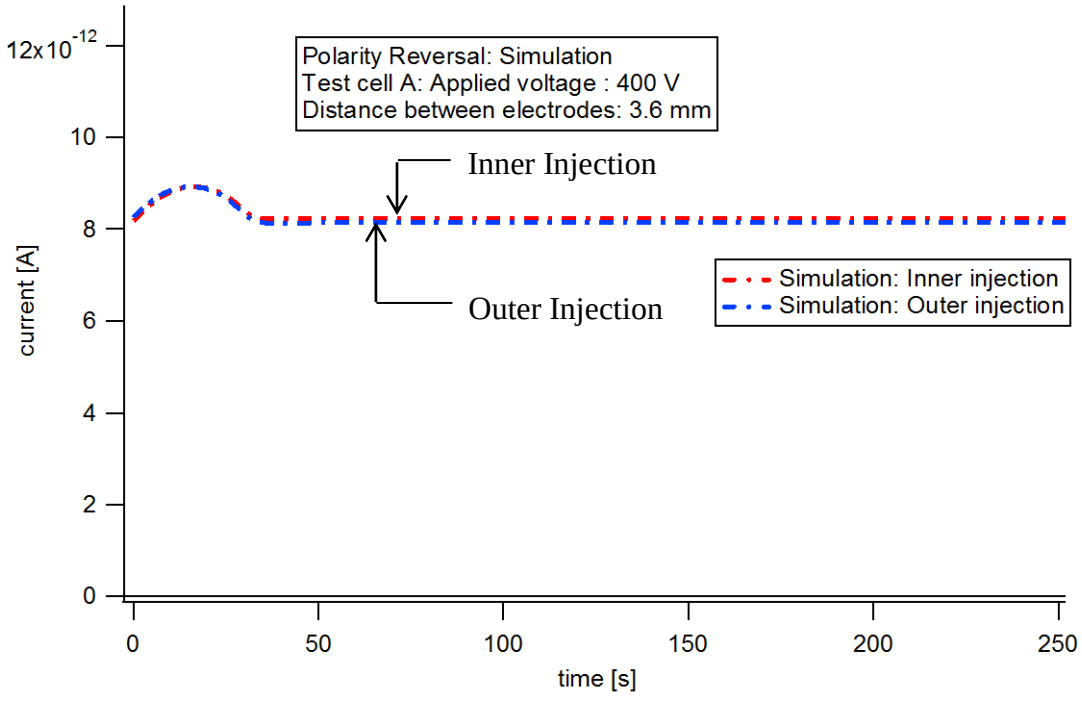

(b)

Figure 30. Measured and simulated currents for polarity reversal method and test cell A the applied voltage is 400 V, oil resistivity of $3 \cdot 10^{13} \Omega$- m.

To evaluate the amount of charges present in oil, the time dependence of the positive and negative currents obtained with polarity reversal method for the test cell A was integrated. The areas under the curves were calculated starting from the time at which the polarity was reversed till the instant that was 10 times of that corresponding to the peak current as mentioned in [8]. Details are provided in the appendix. Figure 31 shows the results for both the positive and negative currents obtained experimentally (Fig. 31a) and from the simulations (Fig. 31b).

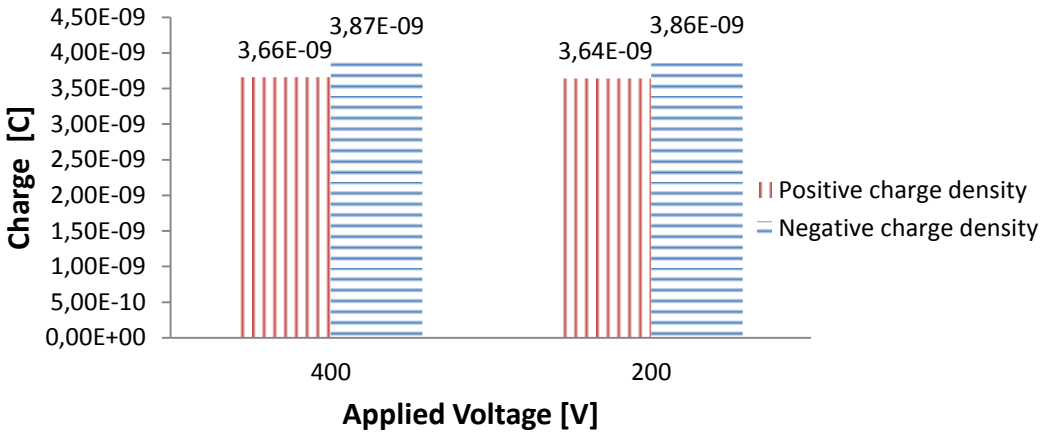

(a)

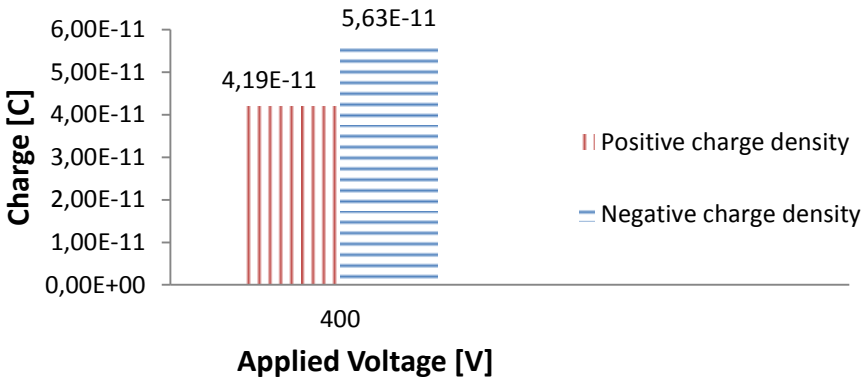

(b)

Figure 31. Charges in oil obtained from experimental (a) and simulated (b) current for polarity reversal method and test cell A.

From the graphs, it can be seen that the area below the curve for the negative current is higher than that below the curve for the positive current. One of the reasons could be a pile up of charges on the electrodes surfaces as explained above.

(c) Time aspects of grounding

Another important phenomenon that was noticed while performing the single polarity measurement was the dependence of the grounding time that resulted in the necessity to keep the test cells grounded for 3 days before performing the experiments, as explained in chapter 5.3. To understand this phenomenon, the simulation results for the restoration times of the system were considered. Figure 32 shows the computated dynamics of the space charges between the electrodes of the test cell B for the applied voltage of 1000 V. In the calculations the oil resistivity was set to 3·1013 Ω-m and ions mobility was assumed to be 10-8 m2/ V-s. As it can be seen the time for the system to reach equilibrium was found to be ~3 hours. However in reality it was in the order of days, i.e. the charges built up in the bulk of oil and at the electrodes (Figure 33) require more time for relaxation. In the simulations, it is assumed that the ions in the bulk of the oil leave the system when reaching the electrode of opposite charge. In the real situation, however, the ions are to be neutralized due to charge transfer reactions, which allow the ionic charge to be transferred to the external circuit. The buildup of charges on the surface of the electrode seems to be more intensive in reality when compared to the simulations. This indicates again that some important processes are missing in the model presented in chapter 2.

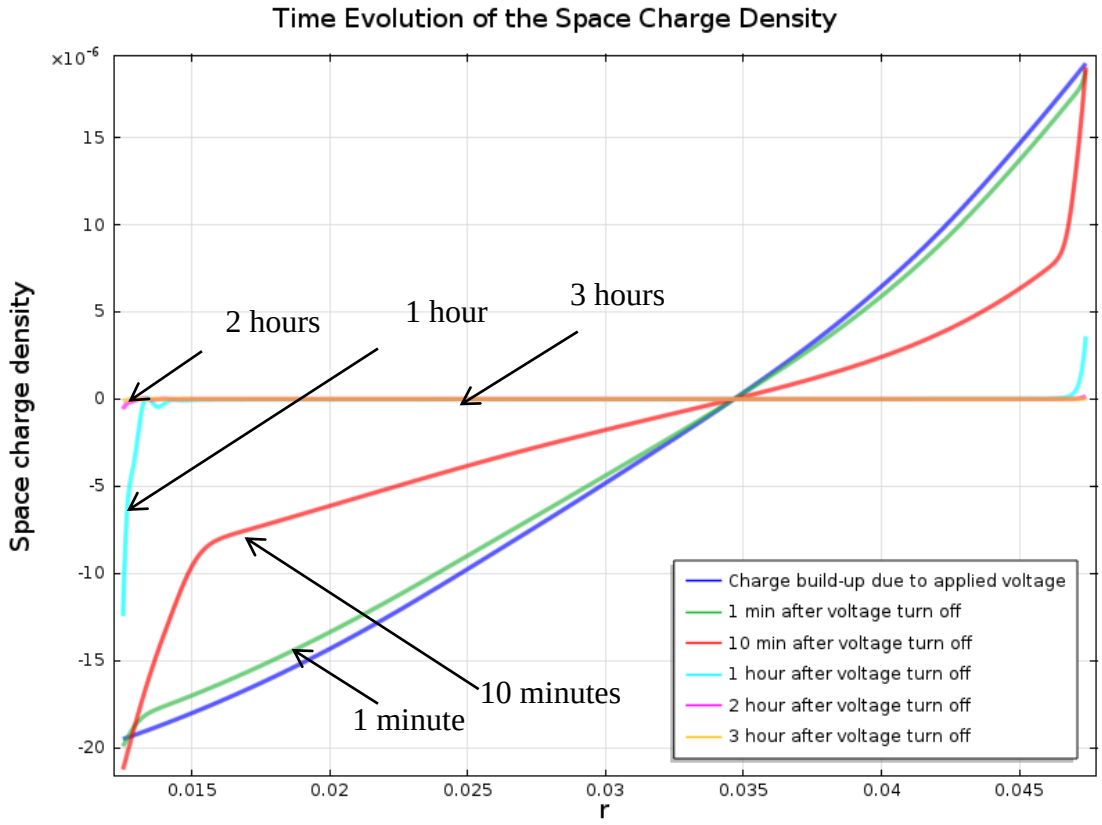

Figure 32. Computed space charge densities for different times in the test cell B.

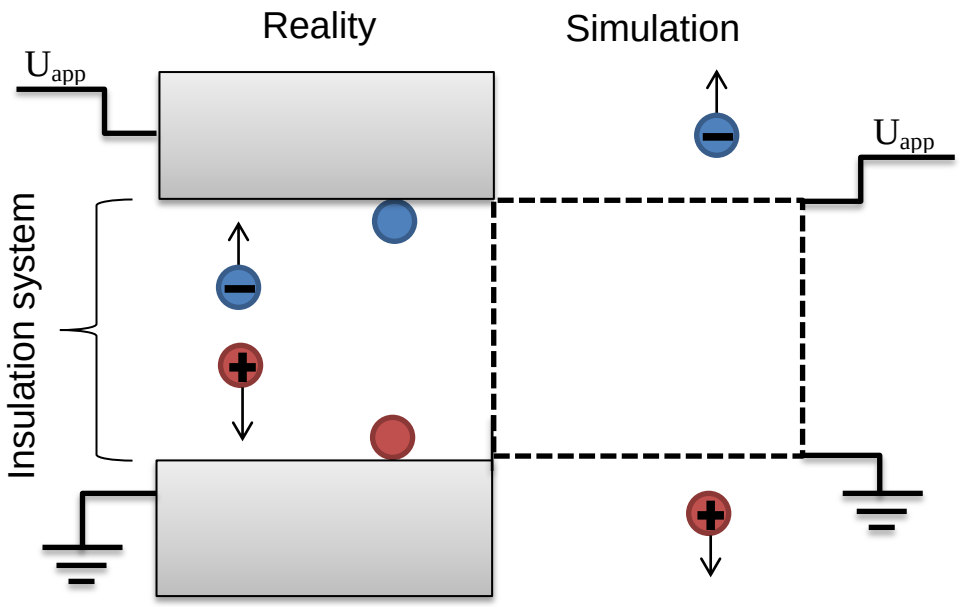

Figure33. Differences between the reality and the simulation model.

6.1 Conclusion

From the experimental results, it was clearly seen that there is a polarity dependence of ion injection. Both the single polarity and the polarity reversal methods clearly show that the positive steady state current was higher than the negative one. Hence the dependence of polarity on injection holds true in both the methods as well. Based on all the obtained results from both the methods, it can be confirmed that the injection is positive in both the test cells irrespectively of the method used for the current measurement.

In the case of polarity reversal, the area under the curve for the negative current (total charge) was higher than for positive current. The reason for a 'bump' in the current in the case of the polarity reversal for test cell A and the large difference in the change in the shape of the positive and negative currents measured with single polarity method in test cell A are still not clearly understood.

One major factor to be considered before performing single polarity measurement is the grounding time of the system which should be long enough to provide reproducible results. The grounding time for the systems used in the present study was found to be around 2-3 days.

6.2 Future work

For better understanding of the injection processes, a lot of additional investigations can be done. Some of them are listed below.

- Investigation of ion injection by adding a metal electrode covered with pressboard.

- Quantifying the level of injection by using a set-up with varying gap distance and performing the same current measurements.
- Investigation of the ion injection with a different material of metal electrode, different oil and geometry.

REFERENCES

1. W. Breuer, D. Povh, D. Retzmann and E. Teltsch, ”Trends for future HVDC Applications”, CEPSI Conference of Electric Power Supply Industry, pp. 1-13, 2006.
2. T. Nara, K. Kato, F. Endo and H. Okubo, “Study on Dielectric Breakdown at DC Polarity Reversal in Oil/Pressboard-composite Insulation System”, Annual Report Conference on Electrical Insulation and Dielectric Phenomena, pp. 588-591, 2009.
3. U. Gäfvert, A. Jaksts, C. Törnkvist and L. Walfridsson, “Electrical Field Distribution in Transformer Oil”, IEEE Transactions on Electrical Insulation, Vol. 27, No.3, pp.647-660, 1992.
4. A. Denat, Etude de la Conduction Electriquedans les Solvants Non Polaires, Thesis L’Universite Scientifque et Medicale et L’Institut National Polytechnique de Grenoble, 1982.
5. A. Denat, B. Gosse and J.P. Gosse, “Ion Injections in Hydrocarbons”, Journal of Electrostatics, Vol. 7, pp. 205-225, 1979.
6. J.O’M. Bockris and A.K.N. Reddy, Modern Electrochemistry 1, Chapter 3, Plenum Press, New York, 1970.
7. J.J. Thomson and G.P. Thomson, “Conduction of Electricity through Gases”, Cambridge University Press, London, 1928.
8. V. Novotny, “Electrical Conduction in Surfactant-Water-Non aqueous Liquid Systems”, Journal of Electrochemical Society, Vol. 133, No. 8, pp. 1629-1636, 1986.
9. A. Ali, A. Denat, J.P. Gosse and B. Gosse, “Creation of charge carriers in Nonpolar Liquids”, IEEE Transactions on Electrical Insulation, Vol. EI-20, No.2, pp.221-231, 1985.
10. U. Gäfvert, O. Hjortstam, Y. Serdyuk, C. Törnkvist and L. Walfridsson, “Modeling and Measurements of Electric fields in Composite Oil/Cellulose Insulation”, Annual report Conference on Electrical Insulation and Dielectric Phenomena, pp. 154-157, 2006.
11. F. Pontiga and A. Castellanos, “Electrical Conduction of Electrolyte Solutions in Nonpolar Liquids”, IEEE Transactions on Industry Applications, Vol.32, No.4, pp.816-824, 1996.
12. P. Langevin, “Recombinaison et mobilites des ions dans les gaz”, Ann. Chimie, Physique, vol. 28, pp. 433, 1903.
13. L. Onsager, “Deviations from Ohm’s law in Weak Electrolytes”, Journal for Chemistry and Physics, Vol. 2, pp. 599-615, 1934.
14. F. O’sullivan, S.H. Lee, M. Zahn, L. Pettersson, R. Liu, O. Hjortstam, T. Auletta and U. Gäfvert, “Modeling the Effect of Ionic Dissociation on Charge

Transport in Transformer Oil", Annual Report Conference on Electrical Insulation and Dielectric Phenomena, pp. 756-759, 2006.

15. A. Castellanos and F. Pontiga, "Generalized Thomson- Onsager model for charge injection into dielectric liquids", CEIDP Annual report, pp. 616-620, 22-25 oct 1995.
16. A. Denat, "Conduction and breakdown initiation in dielectric liquids", 2011 IEEE International conference on Dielectric Liquids.
17. E. Gongadze, A. Iglic, S. Petersen, U. V. Rienen, "An Electrical Double Layer Model with Spatial Variation of the Permittivity", pp. 540-543, 2010 URSI International Symposium on Electromagnetic Theory.
18. D. C. Grahame, "The Electrical Double Layer and the Theory of Electrocapillarity", pp. 441-501, Chemical Reviews, 1947.
19. IR labs, France
20. PAX Diagnostics, USA
21. M.S. Zadeh, "Measurement of Ion mobility in dielectric liquids", Report No. 66/2011, Master Thesis in Department of Materials and Manufacturing Technology, Chalmers University of Technology, 2011.
22. IGOR Pro- www.wavemetrics.com
23. C. Sonehag, "Modeling of ion injection in oil-pressboard insulation systems", Master Thesis in Department of Solid State Electronics, Uppsala University, 2012.

APPENDIX

To evaluate the amount of charges present in oil, the positive and negative currents had to be integrated with respect to time. In the IGOR software, the integration was done by following certain steps. Below are the steps and their respective figures of how the 'area under the curve' was calculated.

Step 1: Select a point A and fix the pointer as shown below. Point B is 10 times the time for the peak current.

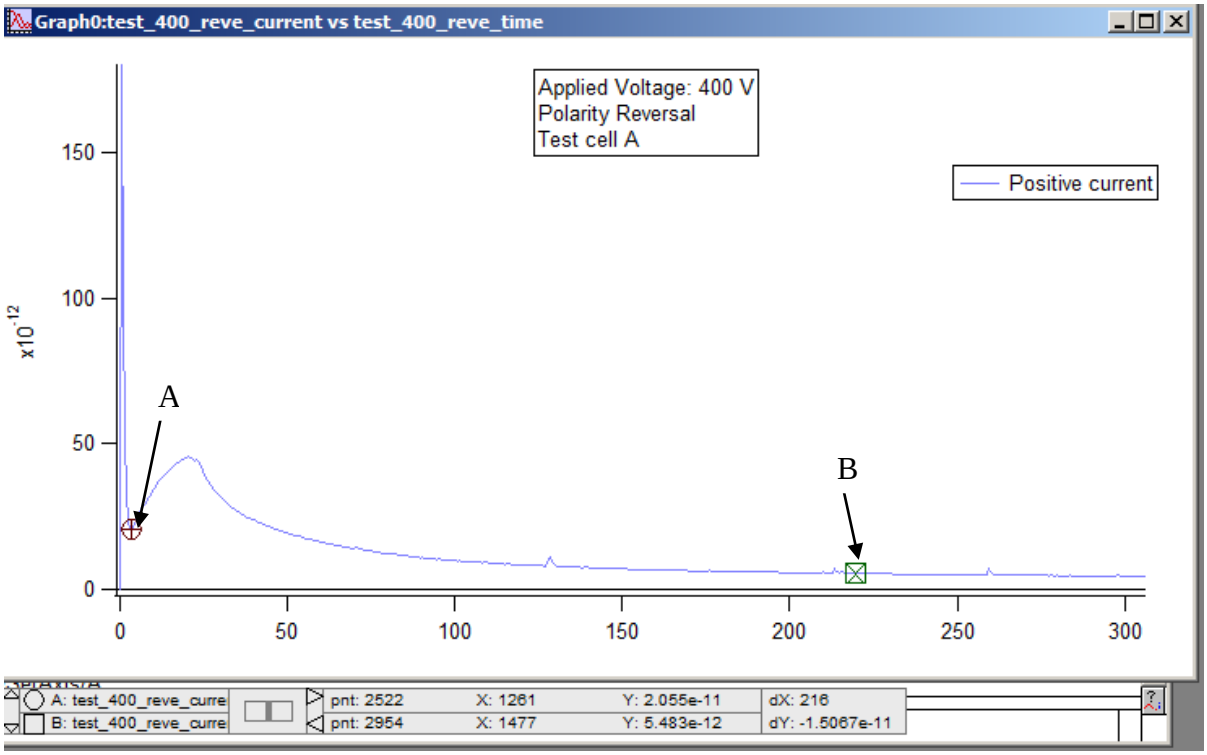

Step 2: Subtract the background to get a curve as shown in the figure below.

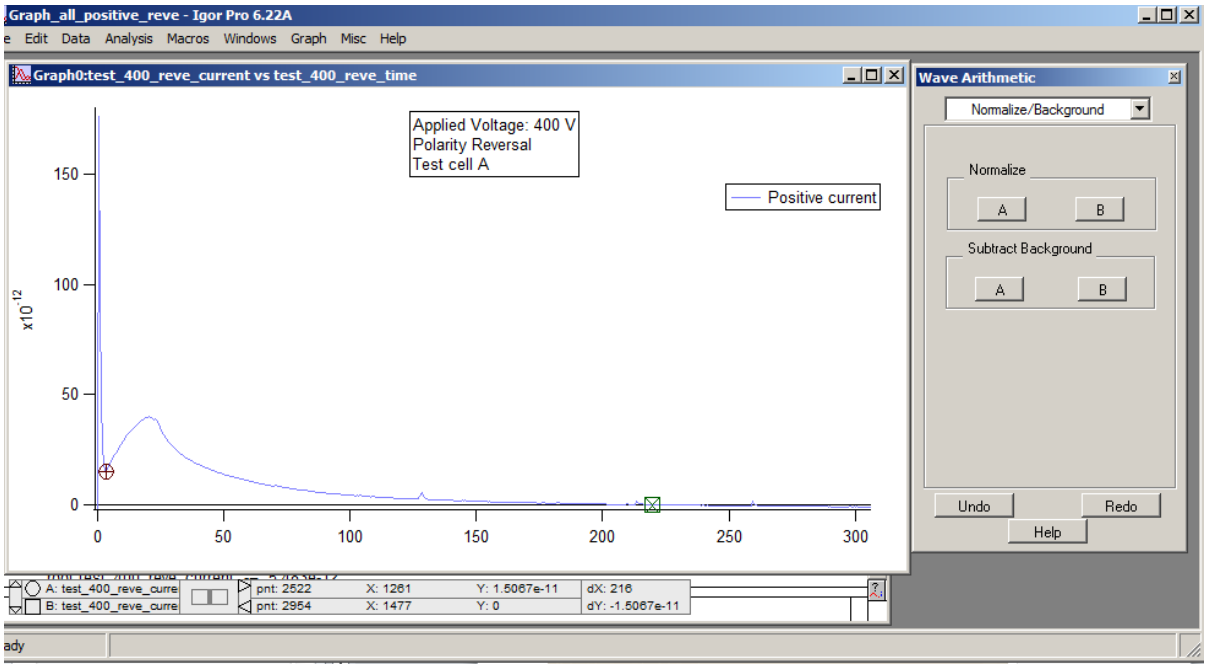

Step 3: Print the area below the curve using **print area** command.

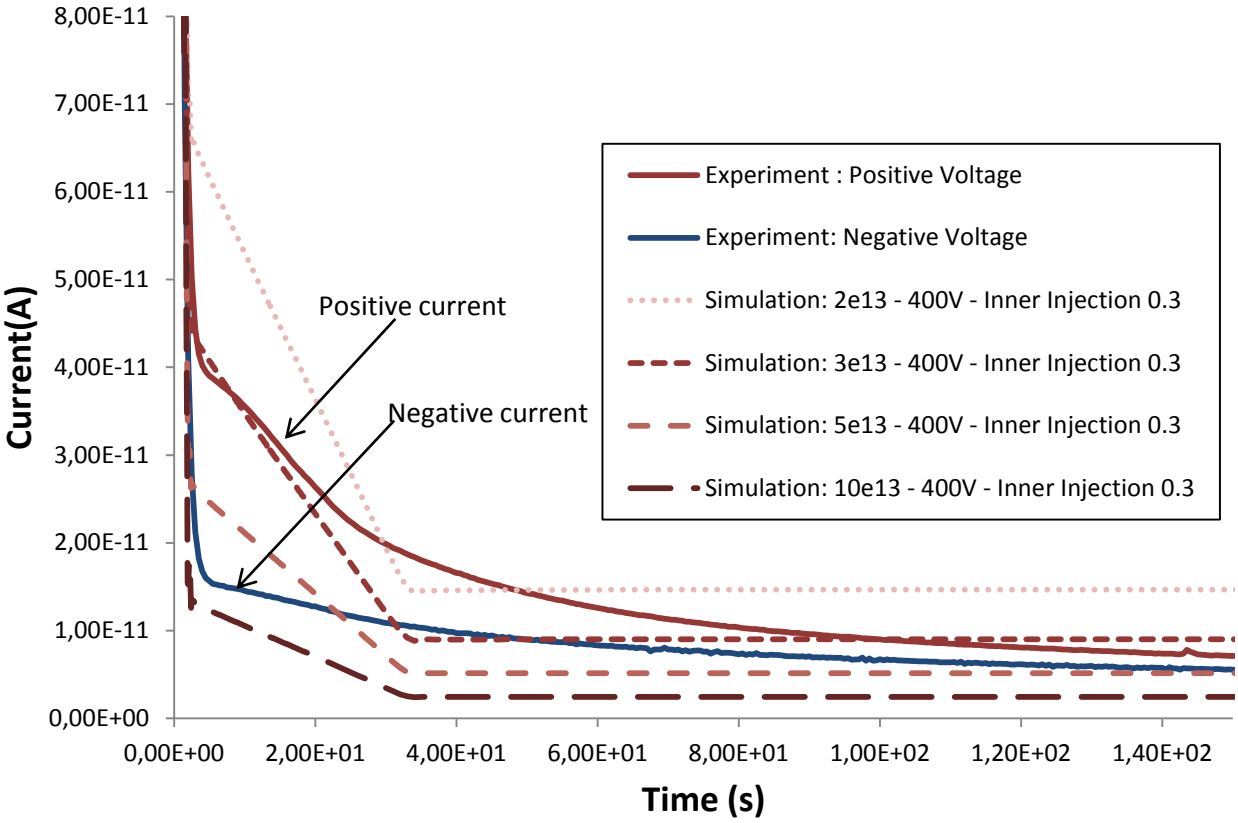

Experimental and simulation results for single polarity method for test cell A with the applied voltage of 400 V for an injection level of 0.3 and different resistivity

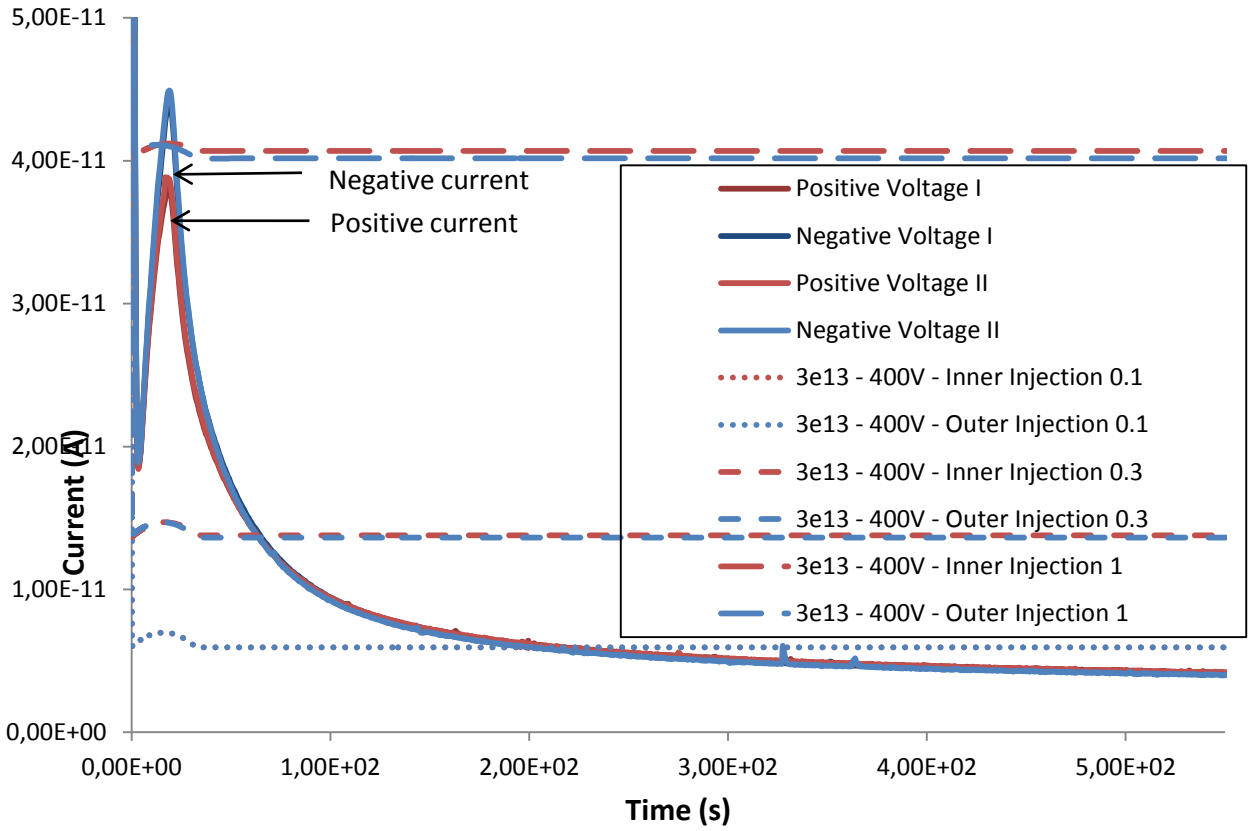

Experimental and simulation results for polarity reversal method for test cell A with the applied voltage of 400 V for a resistivity of $3 \cdot 10^{13}$ Ω-m and different levels of injection